AD-A173 144 EXPERIMENTAL STUDY OF ACTIVE VIBRATION CONTROL(U) 1/1
VIRGINIA POLYTECHNIC INST AND STATE UNIV BLACKSBURG
DEPT OF A.. W L HALLAUER ET AL. 31 JUL 86
UNCLASSIFIED AFOSR-TR-86-1003 F49620-85-C-0024 F/G 22/2 NL

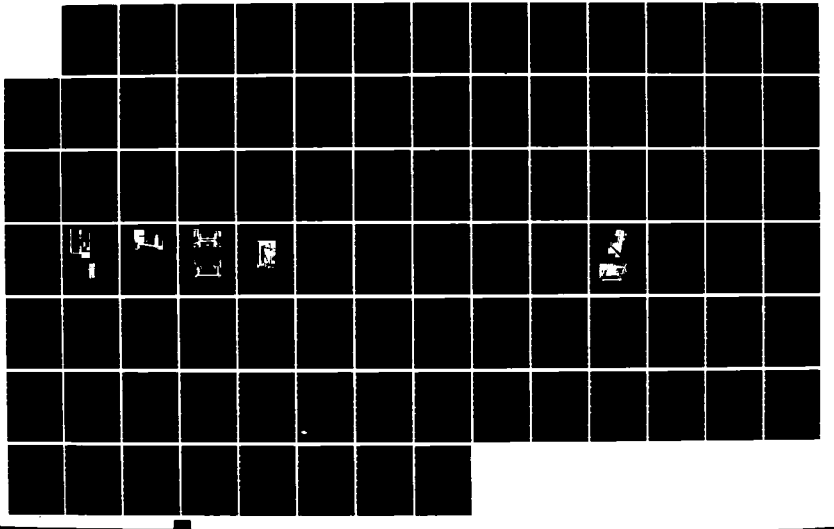

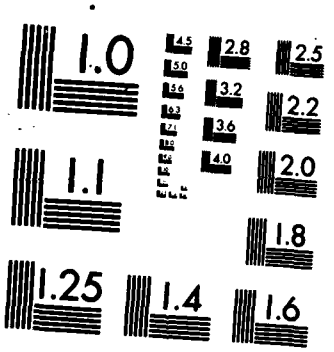

MICROCOPY RESOLUTION TEST CHART
NATIONAL BUREAU OF STANDARDS-1963-A

(2)

ANNUAL TECHNICAL REPORT
TO THE AIR FORCE OFFICE OF SCIENTIFIC RESEARCH
FOR THE PERIOD 1 JANUARY 1985 TO 30 JANUARY 1986

CONTRACT F49620-85-C-0024

AFOSR-TR- 86-1003

EXPERIMENTAL STUDY OF ACTIVE VIBRATION CONTROL*

William L. Hallauer Jr.
Department of Aerospace and Ocean Engineering
Virginia Polytechnic Institute and State University

TABLE OF CONTENTS

*Dr. Anthony Amos is the AFOSR Program Manager.

UNCLASSIFIED

SECURITY CLASSIFICATION OF THIS PAGE

AD-A173 144

REPORT DOCUMENTATION PAGE

1a. REPORT SECURITY CLASSIFICATION: Unclassified	1b. RESTRICTIVE MARKINGS
2a. SECURITY CLASSIFICATION AUTHORITY	3. DISTRIBUTION/AVAILABILITY OF REPORT: Approved for public release; distribution unlimited.
2b. DECLASSIFICATION/DOWNGRADING SCHEDULE	
4. PERFORMING ORGANIZATION REPORT NUMBER(S)	5. MONITORING ORGANIZATION REPORT NUMBER(S): AFOSR-TR- 86-1003
6a. NAME OF PERFORMING ORGANIZATION: Virginia Polytechnic Institute and State University	6b. OFFICE SYMBOL (If applicable): AOE
7a. NAME OF MONITORING ORGANIZATION: Air Force Office of Scientific Research/NA	
6c. ADDRESS (City, State and ZIP Code): Dept. of Aerospace and Ocean Engineering, VPI & SU, Blacksburg, Virginia 24061	7b. ADDRESS (City, State and ZIP Code): Directorate of Aerospace Sciences, Building 410, Bolling AFB, DC 20332
8a. NAME OF FUNDING/SPONSORING ORGANIZATION: AFOSR	8b. OFFICE SYMBOL (If applicable): NA
9. PROCUREMENT INSTRUMENT IDENTIFICATION NUMBER: F49620-85-C-0024	
8c. ADDRESS (City, State and ZIP Code): Bolling AFB DC 20332-6448	10. SOURCE OF FUNDING NOS

PROGRAM ELEMENT NO	PROJECT NO	TASK NO	WORK UNIT NO
61102F	2302	B1	

11. TITLE (Include Security Classification): Experimental Study of Active Vibration Control

12. PERSONAL AUTHOR(S): Hallauer, William L. Jr. ; Kubis, Anthony J. Jr.

13a. TYPE OF REPORT	13b. TIME COVERED	14. DATE OF REPORT (Yr., Mo., Day)	15. PAGE COUNT
Annual	FROM 85-1-1 TO 86-1-30	1986 July 31	87

16. SUPPLEMENTARY NOTATION

17 COSATI CODES		
FIELD	GROUP	SUB. GR

18. SUBJECT TERMS (Continue on reverse if necessary and identify by block number)
Structural dynamics
Active vibration damping (control)
Experimental modal analysis

19. ABSTRACT (Continue on reverse if necessary and identify by block number)

Complementary experimental-theoretical studies were conducted on three separate topics, all of which are related to the dynamics and control of highly flexible large space structures (LSS) in Earth orbit: 1) active damping of vibrations; 2) structural wave propagation; and 3) development of small, flexible laboratory structures having a maneuverable rigid body mode. In the active damping study on a laboratory structure of moderate modal complexity, very good agreement was achieved between experimental measurements and theoretical predictions. The type of active damping applied, output feedback with dual (colocated) control sensors and actuators, should be considered as a candidate for implementation on first-generation LSS because of its stability robustness. The study of wave propagation is focused primarily on transient flexural response of a two-dimensional grid structure to a suddenly applied sinusoidal force at one point. The study is not completed, so results are not presented. New laboratory structures with a maneuverable rigid body mode were built and analyzed. They were relatively simple planar structures composed of thin-walled beam mem-

20. DISTRIBUTION/AVAILABILITY OF ABSTRACT: UNCLASSIFIED/UNLIMITED ☒ SAME AS RPT ☐ OTIC USERS ☐	21. ABSTRACT SECURITY CLASSIFICATION: Unclassified
22a. NAME OF RESPONSIBLE INDIVIDUAL: Anthony K. Amos	22b. TELEPHONE NUMBER (Include Area Code): 202/767-4937
	22c. OFFICE SYMBOL: AFOSR/NA

DD FORM 1473, 83 APR EDITION OF 1 JAN 73 IS OBSOLETE

UNCLASSIFIED

SECURITY CLASSIFICATION OF THIS PAGE

Continuation of block 19. Abstract

bers. They exhibited some unusual dynamic characteristics such as variable natural frequencies, snap buckling, and other nonlinearities. Finite element modeling generally failed to predict the measured vibration modes and the unusual characteristics.

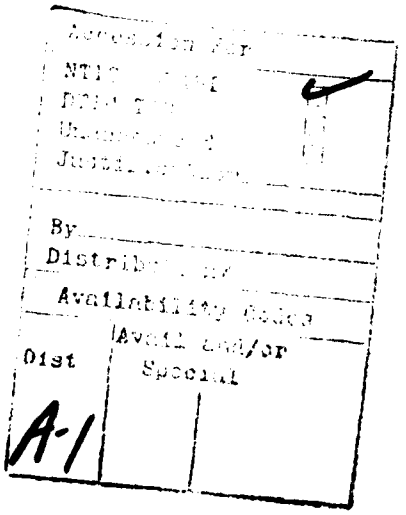

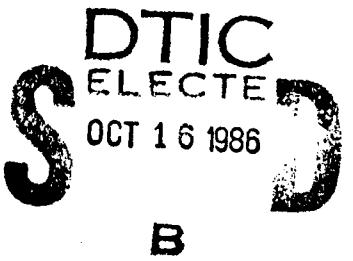

1. INTRODUCTION

The general subjects of this research are the dynamics and control of highly flexible structures, with applications intended for future large space structures (LSS) in Earth orbit.

The research is somewhat unusual inasmuch as its primary emphasis is experimental. The structures that are analyzed experimentally are small laboratory structures not intended to represent any particular LSS, but rather designed to exhibit dynamic characteristics that are generic in various degrees to LSS.

Theoretical analyses are conducted to directly complement the experimental analyses. The theoretical methods are generally state-of-the-art rather than highly innovative. The most important general objective of the research is to achieve satisfactory agreement between experiment and theory, thus validating theoretical concepts for practical application or exposing the reasons why they are inapplicable or ineffective.

The work reported here is continuation of research with AFOSR sponsorship initiated in March 1982.

2. SPECIFIC RESEARCH TOPICS DISCUSSED

Section 3.1 summarizes completed studies of active vibration damping that were natural extensions of earlier work. The research was focused on relatively simple output feedback active damping with the use of dual (colocated) pairs of control sensors and actuators. The actuators were supported externally, not structure-borne. Standard continuous-time control design was analyzed both experimentally and theoretically, and discrete-time design was analyzed theoretically. Additionally, a general evaluation was

made of the potential requirements for and benefits of discrete-time control of LSS.

Section 3.2 summarizes the current status of a continuing study of wave propagation in a laboratory structure.

Section 3.3 reports in detail on the design, testing and theoretical analysis of new, highly flexible laboratory structures intended to have a maneuverable rigid body mode. At least one of these structures will be used in the near future for active control experiments that involve both rigid body and vibration control with the use of structure-borne control sensors and actuators.

3. STATUS OF THE RESEARCH

3.1 CONTINUED STUDY OF ACTIVE VIBRATION DAMPING

3.1.a Coordinated Application of Low-Authority and High-Authority Types of Active Damping

The primary objective of combining high- and low-authority types of active damping is to produce specified damping effectiveness of target (controlled) modes with the high-authority technique while using the low-authority technique to stabilize residual modes that would be driven unstable by the high-authority technique alone. This objective was achieved, but with a method different from the high-authority-low-authority approach originally proposed. We became acquainted with a general type of active damping that is ideally suited to our structural dynamics approach to active suppression of vibrations: Output Velocity Feedback with Dual (colocated and coaxial) sensor-actuator pairs (abbreviated OVFD in the following). OVFD is essentially a high-authority technique that produces damping augmentation in all residual modes, rather than destabilizing them.

It is necessary only that the active damping matrix produced by OVFD be positive semidefinite. For the initial applications of vibration control to LSS, it appears that stability will be of paramount importance, even if it is achieved at the expense of some sacrifice in control effectiveness. Therefore, the author regards OVFD as being a very promising technique for first-generation LSS, and he has elected to pursue this approach.

Experimental measurements on the VPI pendulous plane grid structure have shown OVFD to be very effective. Moreover, the agreement between measurements and theoretical predictions has been very good. The experimental and theoretical analyses are reported in Refs. 1-3. The approach was implemented basically with five dual sensor-actuator pairs. It needs to be emphasized, though, that the translational velocity sensors and the force actuators were externally supported (not structure-borne) devices, essentially without any dynamics of their own to complicate the control task.

The pendulous plane grid structure has 15 vibration modes with natural frequencies under about 13 Hz, and all other modes have natural frequencies above 20 Hz. The OVFD approaches evaluated were designed to produce 10% active damping factors in five target modes, modes 2-6, and these target active damping performances were achieved. Furthermore, OVFD produced substantial damping augmentation in all but two of the residual modes with natural frequencies under 15 Hz and at least some positive damping augmentation in all measurable residual modes.

3.1.b Design and Evaluation of Discrete-Time Digital Control

This study was undertaken by subcontract personnel. The subcontract researchers were initially associated with HR Textron, Inc.; because of a

corporate transaction, their final association was with Sparta, Inc. The research involved two principal tasks, and the results were presented in two separate reports that are appended to this report.

Task 1 was to design and numerically analyze discrete-time control laws for the VPI pendulous plane grid. The results of this task are reported in both Appendices A and B. The approach used in Appendix A was based on a continuous-time control design that had been developed previously by the subcontractor (Ref. 4). The existing continuous-time design was converted by a standard procedure into a discrete-time form appropriate for implementation on a digital controller. This procedure assumes a zero-order hold on the output of the controller, which is common for digital-to-analog converters and, in particular, applies for the PC-1000 array processor used in experiments at VPI. However, the procedure does not account for the inevitable computational delay that a digital controller must introduce. For example, the PC-1000's computational delay is dependent on the sampling period Δt (sec) being used: There is a 1.35 Δt period between the time a signal is sampled by the analog-to-digital converter at the PC-1000's input and the time the associated processed signal appears on the digital-to-analog converter at the PC-1000's output.

In Appendix A, the control design described above is analyzed for four different sampling rates ($1/\Delta t$): 1000, 20, 15, and 10 samples per second. At the fastest rate, the discrete-time control performance is essentially identical to that of the original continuous-time design. At the 20 and 15 sample/sec rates, control performance is somewhat degraded, but the system remains stable. However, at the 10 sample/sec rate an instability appears in the system due to unfavorable interaction between the sampling rate and a particular mode of the pendulous plane grid structure.

The final phase of Task 1 is reported in Appendix B. The objective was to stabilize the 10 sample/sec design discussed above by using discrete-time pole placement analysis. This objective was achieved, but with only a very small margin of stability.

The author's summary assessment of Task 1 is as follows. The subcontractor's theoretical methodology has helped the author to become familiar with the important factors involved in discrete-time control. It must be stated, though, that the quantitative control performances presented in Appendices A and B could not be achieved with the use of VPI's PC-1000 digital controller due to the 1.35 Δt computational delay described above, which is not accounted for in the theoretical analyses. It is quite likely that this important characteristic would render unsatisfactory all of the designs developed for low sampling rates (20, 15, and 10 samples/sec). Unfortunately, the existence of the PC-1000's 1.35 Δt computational delay even at low sampling rates became evident only after the subcontractor had completed Task 1.

Task 2 of the subcontractor was to evaluate the general potential need for and benefits of discrete-time vibration control of LSS. The results of Task 2 are presented in Appendix B. The report discusses the general advantages and disadvantages of analog and digital control, and it makes a strong case for the necessity of digital implementation of vibration control for LSS. The capacity for large numbers of inputs and outputs and the flexibility for quickly modifying control laws are cited as the principal advantages of digital control over analog control. The report cautions, however, that a great deal of progress is required in discrete-time design of multivariable vibration control systems. Moreover, substantial

improvements in processing capabilities of digital controllers are needed to permit sufficiently high sampling rates.

3.2 EXPERIMENTAL AND THEORETICAL ANALYSIS OF WAVE PROPAGATION IN A HIGHLY FLEXIBLE LATTICE STRUCTURE

It was proposed to study experimentally and theoretically traveling waves in the VPI pendulous plane grid structure. Efforts to date have gone primarily into preparation of the theoretical analysis, based on modal analysis using the finite element structural model, and preparation of computer graphics postprocessing required for visualization of traveling wave motion in the structure. Preliminary traveling wave experiments have been run to substantiate the adequacy of the proposed experimental procedure using existing noncontacting force exciters and velocity sensors.

However, extensive experiments have not yet been conducted because it was necessary to modify the pendulous plane grid structure in preparation for planned future active vibration control experiments. In particular, the future control experiments will involve mounting torque-wheel control actuators and relatively large servoaccelerometers on the structure, so extensive modification of its joints was necessary to permit mounting these structure-borne devices.

Since the pendulous plane grid had to be disassembled for the joint modifications, it was appropriate also to take advantage of this opportunity for carefully measuring all members of the structure in order to improve the structure theoretical model. Quantities such as element weights and stiffnesses had previously only been estimated with theoretical formulas based on nominal dimensions and nominal material properties such as density and elastic modulus. More careful measurements showed that some of the

previous estimates were in error by as much as 20%. This careful calibration of the structure is almost complete, so the structure will be reassembled soon and traveling wave experiments will resume. Also, the existing finite element model will be updated to reflect the quantities measured for the structure members.

3.3 DEVELOPMENT OF HIGHLY FLEXIBLE LABORATORY STRUCTURES WITH MANEUVERABLE RIGID BODY MODES

It was proposed to design, build, and test a rotation fixture and two flexible structures, a beam and a plane grid, to be attached to the rotation fixture.

3.3.a Rotation Fixture

The principal parts of the rotation fixture (Figure 1) are a shaft, about 7.5 feet (2.3 m) long, and two bearings to support the shaft vertically, allowing it to rotate about its axis with as little friction as possible. Other parts are brackets and a long-channel-section beam to mount the bearing housings rigidly to the laboratory wall, and attachment fittings to mount the flexible structures onto the shaft. The rotation fixture is shown in Figures 1-3 and some of the subsequent figures. Although the rotation fixture was designed to allow rotation of the shaft about its axis, a shaft clamp (Figure 2) was included to permit complete restraint of the rotation degree of freedom. This clamp was used for the plane grid structure (Section 3.3.c).

3.3.b Rotating Beam-Bar Structure

It was originally intended that a crooked beam structure be attached to the rotation fixture and that the assembly would have a pair of bending-torsion modes with nearly equal natural frequencies. However, it proved to be impossible to design with the materials available a crooked beam structure having closely spaced frequencies.

It was necessary, therefore, to consider an alternate structure design, and the structure shown in Figures 1, 3 and 4 was selected. It consists essentially of the steel rotation fixture and an attached flexible horizontal aluminum beam, to the tip of which is fixed a vertical steel bar. For the lowest few vibration modes of this structure, out-of-plane bending and torsion of the aluminum beam were the dominant structural deformations, and all of the steel parts were effectively rigid. The dimensions and attachment locations of the aluminum beam and steel bar were selected on the basis of a preliminary theoretical analysis to produce a structure having closely spaced second and third natural frequencies. The first mode was rigid body rotation about the shaft axis, with zero natural frequency.

Although the rotating beam-bar structure appears to be uncomplicated, the achievement of reasonable agreement between theoretically predicted and experimentally measured natural frequencies proved to be a difficult task. The first major obstacle was the absence of accurate values for bending and torsion stiffness and inertias of the aluminum beam. As mentioned in Section 3.2, this was a problem with the pendulous plane grid structure as well. Beam inertias were easy to measure, and they turned out to be close to inertias predicted on the basis of nominal dimensions and published density values.

However, accurate beam bending and torsion stiffness were not as easy to obtain. The fundamental problem was the type of aluminum beam used. It was 6061-T6 standard extruded flat stock. Cross-section dimensions of this flat stock, most importantly thickness, vary somewhat from the nominal values. Moreover, actual thickness can be significantly different for two beams having the same nominal thickness if they come from different manufactured lots. Even worse, in some beams the thickness varies significantly across the beam width. Since bending and torsion stiffnesses are proportional to thickness-cubed, the loose tolerance on cross-section dimensions of extruded aluminum flat stock can, indeed, be a source of serious prediction errors.

From the measurements, it must be concluded that another, rather surprising source of errors was modulus of elasticity. Tables in textbooks identify the modulus of elasticity of 6061-T6 aluminum as, typically, 10.0 Mpsi (68.95 GPa). However, values inferred from our static deformation measurements (discussed next) and careful micrometer thickness measurements were on the order of 5% below the typical textbook value.

Considerable time and effort was expended in attempts to measure bending stiffness (EI) and torsion stiffness (GJ) of the extruded aluminum flat stock used for all VPI laboratory models. Because structural vibration frequencies can be measured easily and accurately, initial attempts to determine EI and GJ were free vibration tests. The beam being tested was clamped as rigidly as possible at one end and then excited in either the fundamental bending or the fundamental torsion mode (with the addition of known, rigid tip inertias to depress torsion frequencies). The frequency of response was measured with noncontacting sensors, and this frequency together with measured inertia values was used to infer EI or GJ from well

known formulas for fundamental natural frequencies of uniform, cantilevered beams.

However, it was discovered, unfortunately after a number of these dynamic calibration tests had been run, that a true cantilever boundary condition is very difficult to achieve and that the boundary clamps used had, in fact, permitted significant rotational flexibility at the clamped beam sections. Hence, it was concluded that all stiffness values inferred from the dynamic tests were lower than the true stiffness values and, furthermore, that the stiffness would have to be determined more accurately in static tests with well defined boundary conditions.

The static tests were conducted with the use of a beam analysis frame designed for testing short lengths of thin beams. Weights were used to impose known static loads, and dial displacement gauges were used to measure linear deformations. Figures 5 and 6 are photographs of bending stiffness and torsion stiffness tests. Representative short lengths cut from the extruded aluminum flat stock were tested. With data consisting of the measured loads and deformations, EI and GJ values were inferred from well known strength of materials formulas for static beam behavior.

The second major obstacle to achievement of experimental-theoretical agreement for the natural frequencies of the rotating beam-bar structure was the rotational inertia of the shaft assembly, that is, the rotating portions of the rotation fixture. This inertia was dominated by the steel attachment fittings (Figures 1-4), which were geometrically complicated parts.

An initial attempt was made to determine the shaft assembly inertia experimentally by elastically restraining the shaft and attachment fittings with a known rotation spring, measuring the fundamental free vibration frequency, and calculating the inertia from the single-degree-of-freedom

frequency formula. Unfortunately, the rotation spring used was a short beam clamped to an external support. It was recognized after completion of the test that the clamp had not established a true cantilever boundary condition, as assumed in the analysis. Therefore, the rotational inertia inferred from this dynamic test was incorrect.

Since the first experimental attempt to determine the shaft assembly inertia failed, a painstaking calculation from theoretical formulas was conducted. The calculated value was used in intermediate finite element analyses of the rotating beam-bar structure, as were the statically determined EI and GJ values of the aluminum beam.

Natural frequencies were measured experimentally for both the complete rotating beam-bar structure and the rotating beam alone (with tip steel bar removed). The measured frequencies are listed in Table 1. For each measurement, the structure was excited by hand, then allowed to respond in free vibration. The free vibration response was sensed by four miniature piezoresistive accelerometers, and acceleration signals were fed into a data acquisition-analysis system. Fast Fourier transforms (FFTs) of the time series responses were calculated. Frequencies corresponding to sharp peaks of the FFT magnitudes are the experimental natural frequencies listed in Table 1. Only frequencies well below 15 Hz are listed because the fundamental side bending natural frequency of the shaft assembly was about 15 Hz. It was desirable to model the shaft assembly as rigid in the finite element analysis, so there is no theoretical value corresponding to the actual shaft assembly natural frequency.

In the testing, the structure was usually hand-excited to high levels of response, with the beam tip out-of-plane dynamic translation as much as 2-3 cm from the static position, before the free vibration decay was

measured. The miniature accelerometers allowed this large motion and, in fact, required it to produce strong acceleration signals at low frequencies. A curious phenomenon was observed when the response included substantial rotational vibration of the shaft assembly, as for each mode 2 listed in Table 1: The static rotational position of the entire structure would slowly change during the vibration, coming to rest a short time before vibrational motion had decayed completely. No precise explanation of this rotational wandering was determined, but it must have been caused somehow by nonlinear behavior of the shaft bearings.

For the rotating beam alone, the measured first bending natural frequency was substantially lower than the comparable value from the intermediate finite element analysis. The shaft assembly inertia was a significant parameter for this mode. Since the calculated value of this parameter was highly suspect due to the complicated geometry of the attachment fittings, it was appropriate to adjust the shaft assembly inertia so as to produce agreement between the measured and calculated first bending frequencies of the rotating beam. It was necessary to raise the inertia value 18% above the calculated value.

The adjusted shaft assembly inertia was used in the final finite element models of the rotating beam and beam-bar structures. The finite element models included one degree of freedom (DOF) for shaft assembly rotation and three DOFs for each of eight equally spaced grid points on the aluminum beam. The beam element DOFs were out-of-plane bending translation, bending rotation and torsion rotation. The element stiffness matrices used in the model were the standard beam bending and torsion matrices and, in addition, a geometric stiffness matrix accounting for the influence on out-of-plane stiffness of in-plane static bending moment and shear force imposed

on the thin-walled aluminum beam by weights of the tip steel bar and the beam itself. Standard element consistent mass matrices were used to account for the distributed inertia of the beam.

The calculated theoretical natural frequencies are listed in Table 1 for comparison with the measured values. Reasonable agreement between theory and experiment was achieved. Moreover, the objective of closely spaced second and third natural frequencies of the rotating beam-bar was realized.

However, it must be noted that, despite their close natural frequencies, the second and third modes of the rotating beam-bar were not closely coupled in the sense that they interacted strongly. For example, beating between the two natural frequencies was never observed in the free vibration response. The modes failed to interact because they differed significantly in structural form and inherent damping. Mode 2 was primarily beam bending and shaft assembly rotation, and it was damped somewhat more than usual for a simple bending mode by the shaft bearing friction. Mode 3, on the other hand, was primarily beam torsion and had such small damping that, once set in motion, it would persist for many minutes before finally decaying completely.

Analysis of the rotating beam structures was useful preparation for studying the much more challenging rotating plane grid structure discussed next. However, the rotating beam structures themselves are probably too simple dynamically and too stiff to be of much value in future active vibration control experiments.

3.3.c Floppy Door Rotating Grid Structure

This plane grid is shown in Figures 7 and 8. It was designed to have several two-dimensional out-of-plane low frequency vibration modes, including a zero frequency rigid body rotation mode. No attempt was made to tailor the design so as to produce closely spaced natural frequencies. The structure's shape, flexibility, and rigid body rotational degree of freedom suggest the name "floppy door".

The rectangular perimeter shape shown in Figure 8 was chosen because there was no reason apparent for a more complex geometry. This shape minimizes the chance of introducing errors in the grid point geometry data of the finite element model. Although the structure geometry is symmetric about a horizontal line through joint 3, the vibration mode shapes are not similarly symmetric because the structure's weight causes asymmetric member loading and therefore asymmetric stiffness.

Only one diagonal member was required for truss static stability. However, it was considered undesirable to leave a single long beam only lightly coupled to the rest of the structure, because that member might tend to vibrate in its own nearly isolated fundamental mode. Therefore, two crossed diagonal members were used, and they were connected at joint 3.

The assembly procedure (discussed below) caused the LH and V members to be loaded statically in compression by the structure's weight (see Figure 8 for member abbreviations). It was considered desirable to have at least one beam member in substantial compression relative to its buckling load, both to reduce the overall structural stiffness and to permit the possibility of nonlinear response due to the geometry of deformation. Accordingly, the grid dimensions were chosen so that the LH member, which is most heavily

compressed, would be in static compression equal to about 70% of its Euler (pin-ended) buckling load.

On the basis of extensive experience with the pendulous plane grid structure, it was clear that static gravity-induced loads in the thin-walled members of the floppy door would significantly influence the stiffness and therefore the modes of this structure. These in-plane member loads were used in computation of the geometric stiffness matrix of the finite element model.

In order to make these loads accurately predictable, the floppy door structure was assembled in the following manner to be a statically determinate plane truss for in-plane static response due to gravity loading. First, the LH, UH, V and TD members were attached together, with the bolts at joints 1, 2, 4 and 5 inserted but not tightened. Next, with the bolts still loose, the DWD member was carefully attached to the structure so that its weight was borne equally at joints 2 and 4. Oversized holes were drilled in the DWD member for joints 2 and 3 in order to achieve the desired effect of the DWD member simply adding a dead weight at joint 4 of the LH-UH-V-TD plane truss without accepting any truss loads. Finally, bolted joints 1-5 were carefully hand-tightened. In the bolt tightening process, care was exercised to avoid inducing statically indeterminate loads in the aluminum grid members; however, the members were not instrumented with strain gauges, so there was no way to check for the presence of such unknown loads.

Based on the assumption that the floppy door had indeed been assembled in a statically determinate fashion (for in-plane behavior only, not for out-of-plane behavior), the gravity-induced member loads were predicted from simple hand static analysis. The principal loads were truss tensions and

compressions, with small in-plane bending moments and shear forces in each member (except the vertical member) due only to that member's own distributed weight.

The floppy door structure was tested dynamically both with the shaft free to rotate and with the shaft clamped. The former case is discussed first below.

It proved difficult to measure the natural frequencies and mode shapes of the floppy door with rigid body rotation permitted. In order to produce strong motion signals for the very low frequency vibrations, noncontacting inductive-type proximity probes (Refs. 5-7) were used to sense out-of-plane translation. The tip of such a probe must be positioned at about 2 mm from the static position of the metal surface being measured (a small, thin, steel target taped to the structure), and then the linear range of the instrument is only about ±1 mm of translation from the static position. In initial tests, it was observed that, while vibrating, the floppy door tended to wander statically out of the range of the proximity probes.

Because of the restriction to small vibrational motion, it seems unlikely that nonlinear behavior of the shaft bearings caused the floppy door wandering. In fact, a stable static angular position of the entire structure was found, from which the structure would not wander while vibrating. In this stable position (shown in Figure 7), the grid plane was rotated about 22° from a vertical plane perpendicular to the laboratory wall.

The existence of this stable position suggests strongly that the shaft was mounted with a slight tilt from true vertical (i.e., the direction of gravity), causing a very small pendulum effect. The shaft tilt was measured with a simple pendulum-type inclinometer accurate to about 0.5°. This

measurement showed the tilt to be very small, certainly no more than 0.5°. Such a small tilt is evidently still enough to cause the structure to wander statically toward the stable pendulum position while the structure is vibrating. However, it is evidently not enough to overcome static bearing friction while the structure is still.

Another curious and possibly related phenomenon was observed: The fundamental frequency of the structure was measured to be about 0.26 Hz, not the absolute zero frequency expected for the rigid body mode. The free response of this mode was measured following very gentle blowing excitation near the middle of the vertical member synchronized with the motion. The measured mode shape was rigid body rotation, with any possible deformation being beneath the resolution of the proximity probes.

At first, it seemed that the nonzero frequency of this mode must be the pendulum frequency due to shaft tilt. However, a simple calculation using the reasonably well known inertia properties of the floppy door shows that the tilt would have to exceed 20° to produce the 0.26 Hz frequency. Since the tilt was less than 0.5°, it could not have been responsible.

Also, the following relevant behavior was observed. When the entire floppy door was given a substantial initial rigid body rotational velocity and then released, it would rotate as a rigid body through large angles, gradually slowing down due to bearing friction. It would reach its *maximum* rotation angle, but, instead of stopping at that angle, it would rebound and come to rest after about two cycles of highly damped oscillation (at 0.26 Hz and lower) at an angle slightly less than the maximum. So the stiffness that produced the oscillation must have been highly nonlinear, varying from zero when the structure had substantial rigid rotational velocity to its maximum value only when the rotational velocity was very, very low.

The only possible sources (other than gravity) of the stiffness needed to produce the nonzero frequency appear to be the air and the shaft bearings. However, air usually adds virtual mass and damping, not stiffness, to a very light and flexible structure (Refs. 8 and 9). The 0.26 Hz mode was heavily damped, probably by both bearing friction and air resistance, but it seems very unlikely that air could have added stiffness. Thus, the shaft ball bearings must have been the source of small rotational stiffness.

The possible stiffness generating mechanisms in the bearings seem to be interaction between the balls and their nylon cage and contact elasticity between the balls and races. These mechanisms would seem to be independent of the shaft loading, so it was expected that bearing-induced stiffness should have affected the behavior of the rotating beam structures as well as that of the floppy door. However, careful re-analysis of the rotating beam dynamic data, which had been collected earlier, revealed no evidence of the hypothesized stiffness. Therefore, at this writing the nonzero frequency of the floppy door rigid body mode remains an enigma.

With the shaft rotation only very lightly restrained and with the very limited range of the proximity probes, vigorous hand excitation of the floppy door (as used for the rotating beam structures) was out of the question. Therefore, most testing was done with very low level excitation provided by a noncontacting force actuator at joint 5. The actuator was of the type used previously (Refs. 5 and 7). It consisted of a structure-borne electrical coil (shown in Figure 7) and an externally supported magnetic field structure, which had to be very carefully positioned with its magnetized annular gap surrounding the coil windings.

When initially tried, this actuator was unworkable. The floppy door had been assembled with standard steel bolts. It had been expected that the stray flux of the magnetic field structure would be too weak to attract the bolt at joint 5, but this expectation was wrong. When the actuator was in place with the structure still, the stray flux was too weak to overcome shaft bearing friction. However, when the actuator was providing dynamic excitation, the stray flux would slowly but inexorably draw the joint bolt toward the strong gap magnetic field, thus statically rotating the floppy door out of the range of the proximity probes. The solution to this problem was use of a nonmagnetic 316 stainless steel bolt at joint 5.

Experimental frequency response functions (FRFs) for the floppy door were measured with the use of narrowband incremental sine and broadband swept sine (chirp) force excitation at joint 5. Then natural frequencies and mode shapes were inferred from the FRFs and, in some cases, sine dwells at resonance frequencies. The experimentally determined modes are listed in Table 2. Figure 9 is an example of the FRF graphs from which modal information was inferred.

In the chirp testing, the spectrum of strong excitation and the fast Fourier transform analysis baseband both extended a little beyond 10 Hz. Nevertheless, extensive analysis of the data failed to identify with certainty any modes between 6 Hz and 10 Hz. It seems probable (based upon the theoretical analysis discussed below) that there was at least one mode in the 6-10 Hz range. Perhaps joint 5 was a nodal point of that mode. Unfortunately, it was not possible to test this hypothesis because it was impractical to provide force excitation at any location other than joint 5. The floppy door project was already way behind schedule, and the tasks of

setting up excitation at another location and accounting for it in the theoretical analysis would have consumed a great deal more time.

The experimental data listed in Table 2 were measured in several separate tests intermittently over a period of several months. The deviations indicated from the average frequency values may have been due to several different factors. One certain factor was temperature variation (due to inadequate environmental control in the laboratory), which changed the static member loads. For example, the natural frequency of mode 5 was measured to be 4.99 Hz at a time of normal temperature (about 24°C). Two days later, after a temperature drop of about 5°C, the frequency was measured to be 4.90 Hz. Other possible factors include: limited frequency resolution of the Fourier analysis techniques, which varied (theoretically) from 0.01 Hz to 0.04 Hz; slippage of the bolted joints, allowing member loads to change; and nonlinearity due to compression in the LH member.

When the floppy door was first assembled, it was observed that the compressed LH member was deformed statically by the compressive force. Viewed from joint 5 inboard toward joint 2, the midpoint of the LH member appeared to be bowed leftward by a bit less than one beam thickness. This static equilibrium deformation apparently was the condition required for the occurrence of dynamic snap buckling. As shown on the lower trace of Figure 10, when the vibration amplitude of the LH member exceeded a certain threshold, especially in mode 2, very strong cyclic rightward snapping was observed. No snap buckling was visibly evident when the amplitude was beneath the threshold, but, as indicated by the nonsinusoidal waveform on the upper trace of Figure 10, the response was somewhat nonlinear even without strong snapping. For all modal testing, the level of excitation was

restricted such that dynamic response of the LH member was beneath the snap buckling threshold.

In the finite element model of the floppy door, the shaft assembly was idealized to be rigid and its rotational inertia was assigned the value used finally in the rotating beam finite element models. A small rotational spring (whose physical origin is a mystery - see discussion above) was attached between the shaft assembly and ground to account for the nonzero natural frequency of the first mode; the spring stiffness was chosen iteratively to match the calculated frequency closely with the measured value.

Each major beam member labeled on Figure 8 was divided into four beam finite elements of equal length. Hence, the finite element model included one DOF for shaft assembly rotation and three DOFs at each of sixteen grid points on the aluminum beams, for a total of 49 DOFs. The beam element DOFs were out-of-plane bending translation, bending rotation and torsion rotation. Care was taken to account for the inertias and local stiffening effects of the hardware at the bolted joints.

Standard beam element bending and torsion stiffness and consistent mass matrices were used. As discussed above, the gravity-induced in-plane member loads were expected to have a very significant influence on overall structure out-of-plane stiffness; this influence was accounted for with the use of element geometric stiffness matrices.

Natural frequencies and mode shapes calculated from the finite element model are presented in Table 2 for comparison with experimentally measured data. The agreement between theory and experiment is only fair for modes 1-3 and poor for all higher modes.

To determine if the finite element mesh was sufficiently fine, a coarser model also was analyzed. This model had only two beam finite elements of equal length representing each major aluminum beam member. The modes calculated for this coarser model were only slightly different than the theoretical modes listed in Table 2. This indicated that the modes under 10 Hz calculated for the 49-DOF model were converged for all practical purposes with respect to mesh refinement. Therefore, the poor performance of the finite element model was due to a failure in modeling fidelity rather than inadequate mesh refinement.

The generally mediocre experimental-theoretical agreement was not only a disappointment but also a surprise, since much better agreement had been achieved for the pendulous plane grid (Refs. 1-5), which at least appeared to be a much more complex structure. But the pendulous plane grid was suspended from a horizontal bearing-supported beam, so the initial reaction to the poor agreement shown in Table 2 was suspicion that the vertical shaft assembly (including bearings) of the floppy door was somehow responsible. Hence, the decision was made to test this hypothesis by analyzing both experimentally and theoretically the floppy door structure with the shaft clamped (see Figure 2).

As is described below, the products of these analyses were a great deal of additional information and the general conclusion that the vertical shaft assembly by itself was not responsible for the mediocrity of the experimental-theoretical agreement. However, the clamped-shaft analyses did not reveal with certainty what factor or factors were responsible.

When the shaft was first clamped, it was observed that the static deformation of the aluminum grid was changed by the clamping process. Evidently the clamp did not mate perfectly with the shaft (see Figure 2), so

that the clamping bent the shaft slightly, which, in turn, deformed the aluminum grid. One manifestation of this deformation was that the static bowing of the LH member was no longer substantially leftward, but now slightly rightward. Consequently, the LH member would not exhibit dynamic snap buckling in the clamped-shaft configuration.

More importantly, the shaft clamping process produced additional member loads in the aluminum grid beams. "Additional member loads" were loads added to the basic gravity-induced loads present in the statically determinate plane truss before the bolted joints were tightened. The known basic gravity-induced loads could be accounted for in the finite element geometric stiffness matrices. But the structure became a statically indeterminate plane frame when the bolted joints were tightened, so additional member loads of uncertain origin could not be represented properly in the finite element analysis.

Additional member loads were produced not only by shaft clamping but also by ambient temperature changes. Opportunities arose to measure the effects on natural frequencies of variations in both of these factors. As is discussed in more detail below, it was observed that shaft clamping produced some drastic variations in natural frequencies and that temperature changes produced smaller variations.

With the shaft clamped, the aluminum grid could not rotate rigidly out of range of the proximity probes. Therefore, the structure could be set in motion by fairly vigorous hand excitation, as was used for the rotating beam structures with structure-borne miniature accelerometers. It was much easier to excite the structure by hand than with the force exciter at joint 5 used for the floppy door with shaft free to rotate. Moreover, the structure could be hand-excited at different locations, which would help

preclude the possibility of missing a mode because the excitation was in its nodal region.

Therefore, natural frequencies of this structure were measured as they had been for the rotating beam structures. The structure was excited by hand then released. The free vibrations following excitation were measured, and FFTs of the responses gave spectrum graphs, the peak magnitudes of which are at the modal natural frequencies. The measured natural frequencies for several different cases are listed in Table 3. Figure 11 is an example of the spectrum graphs from which the natural frequencies were inferred.

Comparison of the first two cases in Table 3 shows the influence of temperature change on the natural frequencies. The opportunity for making this comparison was afforded by a combination of poor temperature control in the laboratory and a succession of unusually cold winter days. As shown in Table 3, a 9°F (5°C) temperature change caused natural frequency changes as much as 0.15 Hz.

It was desirable to evaluate the temperature influence in greater depth, so an appropriate finite element analysis was conducted. With the structure modeled as a plane frame, the static additional member loads produced by temperature change were calculated. The resulting loads were surprisingly large in comparison with the gravity-induced member loads. Calculated axial forces (tensions and compressions) due to both temperature change and gravity are listed for example in Table 4. According to these values, a temperature rise of only 4°F (2.2°C) would nullify the gravity-induced compression and tension, respectively, in the LH and TD members.

In view of the large additional member loads due to temperature change, one might expect even greater differences between case 1 and case 2 natural frequencies than is shown in Table 3. Evidently the differences are not

greater because any temperature change would stiffen some members of the aluminum grid but soften some others, and these opposite effects would at least partially cancel each other. It would be appropriate to test this hypothesis with finite element calculations of natural frequencies versus temperature, but these calculations were not made.

Comparison of cases 2 and 3 in Table 3 shows the effect on natural frequencies of the additional member loads induced by clamping of the shaft. After data was taken for case 2, the aluminum grid structure was dismantled and then re-assembled by the procedure described above for allowing only statically determinate gravity-induced loads in the aluminum beam members. When the bolted joints were loosened in the dismantling process, it was observed that substantial in-plane loads were relieved. This was direct proof that shaft clamping had inadvertently stressed the structure.

There were substantial differences between almost all of the corresponding case 2 and case 3 natural frequencies. The most remarkable result of the in-plane load relief for case 3 was the emergence of a pair of modes, the fourth and fifth, with very closely spaced natural frequencies. These modes are discussed in more detail below.

From comparison of cases 2 and 3, one learns two important lessons relative to future use of the floppy door structure (for, e.g., active control experiments). First, in-plane loads do, indeed, significantly influence at least the low frequency modes. Second, if the shaft is to be clamped, then the clamping must be done in a manner that does not produce unknown in-plane loads in the aluminum beams. Such loads cannot be represented in the finite element structural model.

Table 3 shows that the conditions of cases 4 and 5 were very similar to those of case 3, and that, with one exception, the measured natural frequencies were also very similar.

The exception is the frequency of mode 2, which was a global twisting mode very similar to mode 2 of the structure with shaft free to rotate (see Table 2). The structure was dismantled and re-assembled between cases 4 and 5, and the second natural frequency dropped from 1.12 Hz to 1.00 Hz. Mode 2 involved substantial bending of the highly compressed LH member, so its frequency was probably sensitive to the amount of compression. The drop in frequency suggests, therefore, that the compression was greater in case 5 than in case 4. If so, then the compression must have been affected significantly by the bolt tightening procedure. This procedure was not conducted identically during each re-assembly of the structure because it had been presumed benign relative to member loads.

Due to bolt tightening, temperature changes, and perhaps other unknown factors, the in-plane member loads were possibly not as predictable as had been expected. Since these loads significantly affect the stiffness of this thin-walled structure, it may be desirable in future experiments on the floppy door to monitor member loads with strain gauges.

By additional testing beyond that reflected on Figure 11, it was determined that modes 4 and 5 of cases 3-5 not only had close natural frequencies, but were, indeed, closely coupled. This coupling is clearly evident in the free vibration time history of Figure 12. This is the greatest degree of modal coupling that the author has ever observed in a relatively simple laboratory structure. It occurred by chance and, unfortunately, is probably not easily reproducible.

The finite element model of the structure with shaft clamped was the same as that of the floppy door, except that the DOF for shaft assembly

rotation was fixed. The natural frequencies calculated with this theoretical model are listed on Table 3. There is fair agreement between the lowest four theoretical frequencies and the corresponding values of experimental cases 3-5. However, even this small success becomes tarnished when one compares mode shapes. It is difficult to infer accurate information on experimental mode shapes from spectrum graphs such as Fig. 11. Nevertheless, it was determined by various means, including direct visual observation, that experimental-theoretical mode shape agreement was poor for all but the first two modes.

Extensive dynamic analysis of the floppy door structure had not revealed with certainty the factor or factors responsible for the poor performance of the theoretical finite element models. It was decided, therefore, to conduct another type of experimental-theoretical analysis, this time a static analysis, in search of modeling errors.

Since the structure had been designed such that the LH member would be in substantial compression relative to its Euler buckling load, it seemed appropriate to conduct a static stability analysis. The specific structure studied is shown in Figure 13. The DWD member was removed from the complete structure, leaving the four-bar structure shown. This structure was unquestionably determinate in its plane, at least before the joint bolts were tightened. The shaft was clamped (with joint bolts loosened) to prevent the structure from wandering rigidly.

The structure was loaded with a variable weight attached at joint 4. This simulated the loading that the DWD member imposed on the complete floppy door structure. A simple weight hanger was designed to keep the weight always directly beneath joint 4 without impeding deformation of the structure. The weight hanger, shown in Figures 13 and 14, consisted of the

following: a long nylon string with small nooses at each end, one looped around the bolt head at joint 4 and the other looped around the nut opposite to the bolt head; a 15-inch (0.26 m) length of 0.5 inch (13 mm) square aluminum tube, through which the string was threaded; and a small hook screwed into the center of the tube, to which weights were attached via short wires.

When weights were hung slowly from the structure, it deformed into a global twisting shape (similar to the shape of mode 2 in Tables 2 and 3), with joint 4 displaced leftward and joint 5 rightward (from the viewpoint of Figure 13). The aluminum bar of the weight hanger served to spread the nylon string away from the vertical member of the structure. The vertical member deformed into contact with the string only when the hung weight exceeded 5.5 lb (2.5 kgf), which, therefore, was the maximum weight for which data were collected.

For theoretical static stability analysis of the structure in Figure 13, a finite element model was developed. This model had the same mesh refinement as the models used for dynamic analysis, namely, four beam finite elements per each major structure member. The buckling weight at joint 4 calculated from an appropriate eigenanalysis of this finite element model was 4.17 lb (1.89 kgf). The corresponding buckling mode shape was global twisting as described above.

Experimental static stability analysis was conducted carefully with use of the weight hanger and stationary rulers adjacent to joints 4 and 5 that permitted visual measurement of out-of-plane joint translations. The basic translation versus weight data is shown on Figure 15. Plotted on the graph are absolute translations of each joint and their sum, which is the translation of the two joints relative to each other.

Shown on Figure 16 are Southwell plots of the data from Figure 15. A Southwell plot, as described in Ref. 10, is intended to permit inference of a critical buckling load from subcritical data. If the data were suitable for this interpretation, each plot of Figure 16 would have a straight-line asymptote at low values of the ordinate, and the three asymptotes would be parallel to each other. The critical buckling load would be the slope of these asymptotes.

Unfortunately, the data are quite unsuitable for inference of an experimental critical buckling load. It should be noted that all accurately measured out-of-plane translations were very large relative to the aluminum beam thickness of only about 3 mm. In contrast, most buckling experiments on thin-walled structures involve deformations only on the order of the thickness (Ref. 10). It seems possible, therefore, that the unloaded geometry of the aluminum grid was so imperfect as to permit extremely large out-of-plane deformation for even very small in-plane loads. If so, then the unloaded grid may not have been sufficiently planar to exhibit bifurcation buckling. Further evidence of substantial out-of-plane imperfection is discussed below.

It is clear that the static stability study failed, as had the dynamic studies, to culminate in satisfactory experimental-theoretical agreement. Nevertheless, the study was useful for revealing the possibility of out-of-plane grid imperfection and for demonstrating another unexpected phenomenon: Slippage of the bolted joints. Before the data shown on Figure 15 were measured, the structure was loaded with weights attached to the hanger in the following sequence: 0, 1, 3, 5, 5.5, 1, 0, 2, 3, 6 lbs. The out-of-plane translations measured for the second occurrences of 0, 1, and 3 lbs loading were substantially different than those for the first occurrences.

That is, the structure was not behaving repeatably. It seems likely that this behavior was caused by slippage of the joints, even though the bolts had been thoroughly tightened. Loading with the 6-lb weight seemed to settle the structure. Measurements made after that time were quite repeatable and, in fact, produced the data shown on Fig. 15. But the strong evidence of joint slippage during the static testing at least suggests the possibility that this may have occurred during dynamic testing as well, allowing member loads and consequently structural modes to vary.

After the completion of static stability testing, the structure was restored to its original configuration (complete floppy door with shaft free to rotate - Figure 7). The visual appearance had not changed relative to earlier testing, but closer attention was paid now to a detail that had been observed earlier but judged irrelevant: Both the UH and TD members were bowed leftward by as much as 2-4 thicknesses at their midpoints (viewed from outboard toward the shaft). This suggested that the upper and lower attachment fittings were out of alignment, with the upper pointing leftward of the lower. When the floppy door was assembled for the very first time, alignment of these fittings was attempted with a fairly crude plumb bob, but that alignment had apparently been inadequate.

Therefore, at this much later date, the attachment fittings were re-aligned in a different manner: The upper fitting was loosened on the shaft and rotated slightly rightward until both the UH and TD members were as straight as could be achieved by manual adjustment and visual observation. The LH member was observed to be bowed slightly more leftward after the re-alignment than it had been before. The maximum leftward bowing of the LH member now was perhaps 1+ thickness at its midpoint.

The slight, simple re-alignment produced some remarkable and positive results. It would have been impractical to repeat completely the dynamic testing that gave the data in Table 2, but time was taken for some very simple testing and observations. With the use of gentle hand and blowing excitation, modes 1 and 2 were observed. Proximity probes to measure the motion were positioned at joint 2 and at the midpoint of the LH member.

Mode 1 was observed to be unchanged by the re-alignment. This was expected since motion in mode 1 was only rigid body rotation.

However, mode 2 was changed dramatically. The very last testing of the structure before re-alignment of the attachment fittings had produced the oscilloscope records of Figure 10. From the upper trace of Figure 10, one observes that there was substantial joint 2 motion in mode 2 and that, at the lowest levels shown, the waveform had a crest-trough shape with frequency of 1.00 Hz. After the re-alignment, the natural frequency rose to 1.31 Hz, the joint 2 motion became imperceptibly small on the scale of Figure 10, and the waveform of motion at the LH member's midpoint was very nicely sinusoidal, with no hint of the crest-trough shape. Moreover, it was still possible to drive the LH member into dynamic snap buckling, but only at motion amplitudes much higher than those of Figure 10.

The new experimentally measured mode 2 was almost identical to the theoretically predicted mode 2 listed on Table 2. It appears that earlier misalignment of the attachment fittings had warped the grid structure into such a non-planar shape as to couple shaft rotation with the global twisting motion; the shaft assembly inertia evidently caused the measured natural frequency to be much lower than predicted theoretically on the basis of a perfectly planar finite element model.

Unfortunately, this reasoning fails to explain the low mode 2 frequencies measured before re-alignment for the grid structure with shaft clamped (Table 3). Also, it would be reckless to speculate how the re-alignment affected the higher modes of the floppy door. Complete re-testing is required to provide that information.

A summary is in order of the principal lessons learned from the time-consuming and difficult analysis of the floppy door. These lessons should be recalled in future experimental applications of the structure. Ranked roughly in order of importance, the lessons are:

1. Misalignment of the attachment fittings throughout most of the testing was probably a serious liability. With the fittings now better aligned, the floppy door modes should be measured again to determine if there is general improvement in experimental-theoretical agreement.
2. Variations of in-plane member loads were clearly important. After shaft clamping and/or temperature changes, the bolted joints should be loosened and then re-tightened to relieve all but the gravity-induced loads. However, it is possible that the bolt tightening process and/or slippage in the joints may make the calculated statically determinate loads incorrect. Therefore, it may be necessary to monitor the member loads with strain gauges.
3. The rotational inertia of the shaft assembly (sans aluminum grid) should be measured. It should be possible to do so with a simple low frequency incremental sine shake test of the shaft assembly without any restraining spring.
4. Nonlinear behavior of the ball bearings supporting the shaft was observed occasionally during the testing, but it is probably not important. Bearing-induced rotational wandering occurred only at much

higher vibration amplitudes than would be permitted in an active control experiment. Bearing friction appeared to be slightly but not disruptively nonlinear. Finally, the extremely small nonlinear rotational stiffness caused apparently by the bearings also appeared to be harmless. It is possible that this stiffness might be eliminated entirely by loosening the bearing nuts.

4. PUBLICATIONS AND CONFERENCE PAPERS

References 5 and 6 were published. References 2 and 3 were presented and published in conference proceedings.

5. PROFESSIONAL PERSONNEL

VPI Personnel:

Principal Investigator: William L. Hallauer Jr.

Graduate Research Assistants:

Gary R. Skidmore: Ph.D. degree received June 1985, Ph.D. dissertation listed as Ref. 1; presently employed by Martin Marietta Denver Aerospace of Denver, Colorado

George C. Schamel III: M.S. degree received March 1985, M.S. thesis listed as Ref. 7; presently employed by DEI Tech, Inc. of Hampton, Virginia

Dinesh Trivedi: Ph.D. candidate

Sparta, Inc. Personnel:

Project Director: Richard Quartararo

Research Engineer: Anthony J. Kubis, Jr.

REFERENCES

1. G.R. Skidmore, "Experimental-Theoretical Study of Velocity Feedback Damping of Structural Vibrations," Ph.D. dissertation, VPI&SU, May 1985.

2. W.L. Hallauer Jr. and G.R. Skidmore, "Active Vibration Damping Experiments at VPI&SU: Overview and Recent Results," Fifth VPI&SU/AIAA Symposium on Dynamics and Control of Large Structures, Blacksburg, VA, June 1985; Proceedings, pp. 437-454.

3. G.R. Skidmore and W.L. Hallauer Jr., "Experimental-Theoretical Study of Active Damping with Dual Sensors and Actuators," AIAA Paper No. 85-1921-CP, AIAA Guidance, Navigation, and Control Conference, Snowmass, CO, August 1985; Collection of Technical Papers (AIAA CP856), pp. 433-442.

4. W.L. Hallauer Jr. and A.P. Nayak, "Experimental Study of Active Vibration Control," Final Technical Report for AFOSR Contract F49620-83-C-0158, 13 February 1985.

5. W.L. Hallauer Jr., G.R. Skidmore and R.N. Gehling, "Modal-Space Active Damping of a Plane Grid Structure: Theory and Experiment," Journal of Guidance, Control and Dynamics, Vol. 8, No. 3, May-June 1985, pp. 366-373.

6. G.R. Skidmore and W.L. Hallauer Jr., "Modal-Space Active Damping of a Beam-Cable Structure: Theory and Experiment," Journal of Sound and Vibration, Vol. 101, No. 2, 22 July 1985, pp. 149-160.

7. G.C. Schamel II, "Active Damping of a Structure with Low-Frequency and Closely-Spaced Modes: Experiments and Theory," M.S. thesis, VPI&SU, March 1985.

8. C.V. Stahle, "Analysis and Testing of Large Space Structures," pp. 114-121 in NASA Conference Publication 2258, Modeling, Analysis and Optimization Issues for Large Space Structures, 1983.

9. J.-N. Juang and L.G. Horta, "Effects of Atmosphere on Slewing Control of a Flexible Structure," AIAA Paper No. 86-1001-CP, 27th AIAA Structures, Structural Dynamics and Materials Conference, May 1986.

10. J.G. Croll and A.C. Walker, Elements of Structural Stability, Halsted Press, 1972, pp. 82-90.

Table 1

Experimental and theoretical modes of the rotating beam structure and rotating beam-bar structure

Mode	Natural Frequencies (Hz) Experimental	Theoretical	Mode Description
Rotating beam			
1	0	0	Rigid body rotation
2	4.57	4.57	First bending, with much rotation of shaft assembly
3	12.03	12.38	Second bending
Rotating beam-bar			
1	0	0	Rigid body rotation
2	3.24	3.29	Predominantly beam bending, with much rotation of shaft assembly; damping higher than usual due to friction in shaft bearings
3	3.47	3.40	Predominantly beam torsion, with very little rotation of shaft assembly; damping extraordinarily low; nodal point on tip bar about 4" (0.1 m) below elastic axis of aluminum beam
4	9.89	10.08	Predominantly beam bending; damping normal

Table 2

Experimental and theoretical modes in the 0-10 Hz range of floppy door structure with shaft free to rotate

	Natural Frequencies (Hz)		
Mode	Experimental	Theoretical	Mode Description*
1	0.26 ± 0.02	0.27	Nearly rigid body rotation, with only slight deformation; high damping
2	1.08 ± 0.08	1.27	Global twisting (joint 4 out of phase with joint 5), with very little rotation of shaft assembly; low damping
3	3.01 ± 0.04	2.87	Bending (joints 4 and 5 in phase), with much rotation of shaft assembly (joints 1 and 2 out of phase); high damping due to friction in shaft bearings
4	4.24	4.20	
5	4.94 ± 0.05	5.93	
6	5.95 ± 0.05	6.37	
7	-	9.30	

*Only three motion sensors, one at each of joints 2, 3 and 5, were used experimentally to detect mode shapes. These sensors sufficed to show that the simple (and visually observable) shapes of measured modes 1-3 agree well with their theoretically predicted counterparts. However, the remaining mode shapes are more complicated spatially. The sensors used were adequate only to demonstrate substantial differences between experimental and theoretical shapes of the higher modes, even for mode 4, for which the experimental and theoretical frequencies are nearly coincident.

Table 3

Experimental and theoretical natural frequencies in the 0-10 Hz range of the floppy door structure with the shaft clamped

Case	Natural Frequencies (Hz) 1	2	3	4	5	6	Changes Relative to Previous Case
Experimental (listed in chronological order)							
1*	0.57	1.22	3.66	4.47	5.06	7.12	Not applicable
2	0.60	1.16	3.76	4.32	5.20	7.12	9 days later, temperature normal, that is, about 5°C higher than for case 1
3	0.56	1.08	3.52	4.70	4.76	7.56	All joints loosened then retightened
4	0.56	1.12	3.52	4.70	4.79	7.48	3 days later, temperature about 1°C higher
5	0.56	1.00	3.48	4.66	4.78	7.52	All joints loosened then retightened
Theoretical							
	0.63	1.27	3.59	4.61	6.07	6.91	Not applicable

*The joints were initially tightened with the shaft free several weeks prior to Experimental case 1 during a time of normal temperature in the laboratory. Case 1 was run on a very cold day, resulting in thermal additional member loads. Also, for case 1 the additional member loads produced earlier by clamping (and incidentally bending) the shaft had not been relieved by loosening and then retightening all joints.

Table 4

Calculated average static axial forces in the aluminum beam members of the floppy door structure

Member	Calculated Average Static Member Axial Force	
	Temperature-Induced Force (lb/°F)	Gravity-Induced Force (lb)
LH	+1.50	-5.90
V	+1.47	-2.81
TD	-2.09	+8.25
DWD	-2.09	0.00
UH	+1.50	0.00

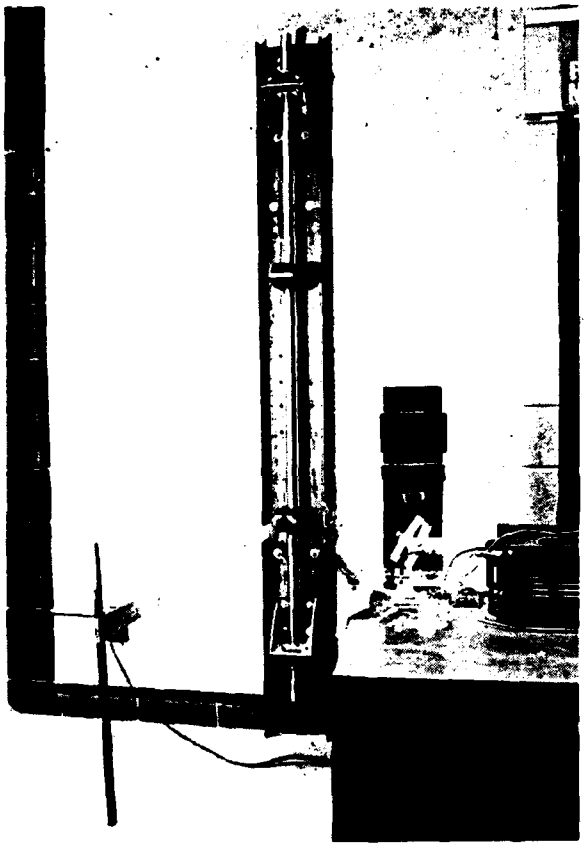

Figure 1

Rotation fixture (at center) with beam-bar structure mounted on lower attachment fitting. The shaft clamp is not attached, so the shaft is free to rotate.

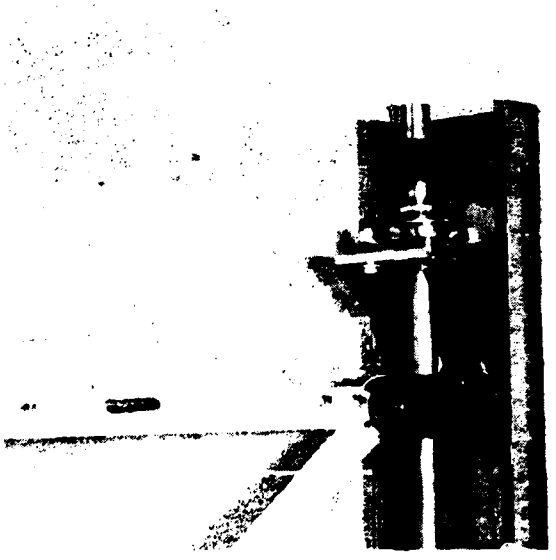

Figure 2

Top portion of rotation fixture with shaft clamp attached just below top of shaft. Also shown are the upper bearing bracket and the upper attachment fitting holding one joint of the floppy door structure.

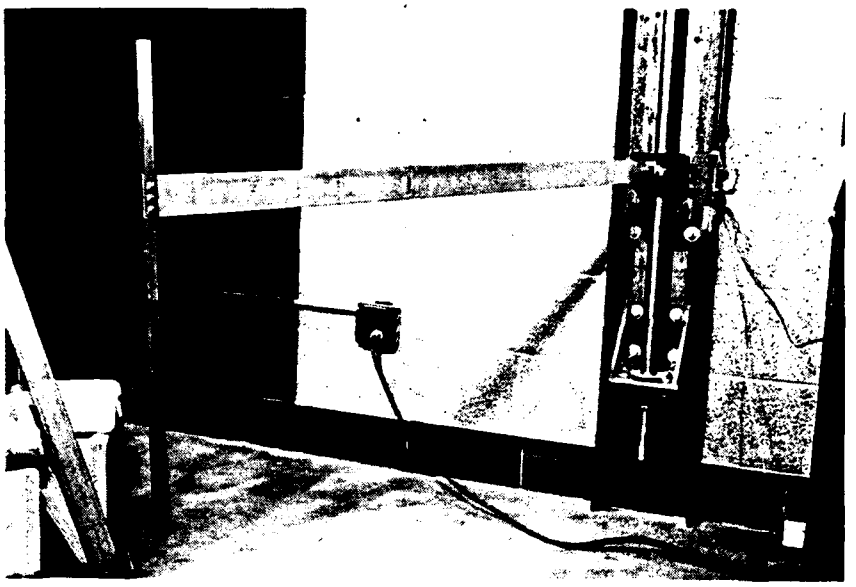

Figure 3

Photograph of rotating beam-bar structure, with vertical rigid steel bar at left, horizontal aluminum beam in center, and lower portion of rotation fixture at right.

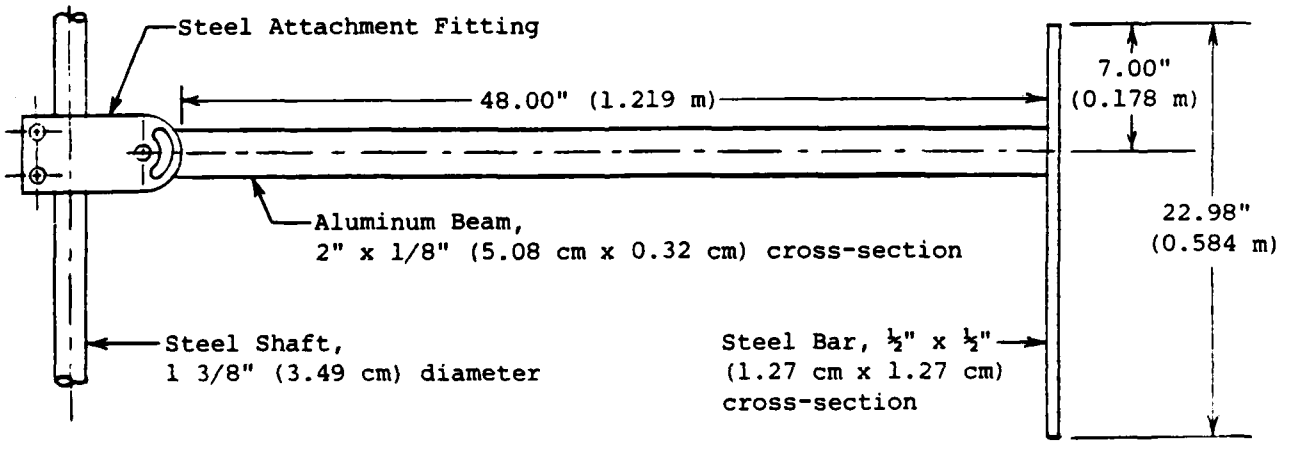

Figure 4

Line drawing of rotating beam-bar structure.

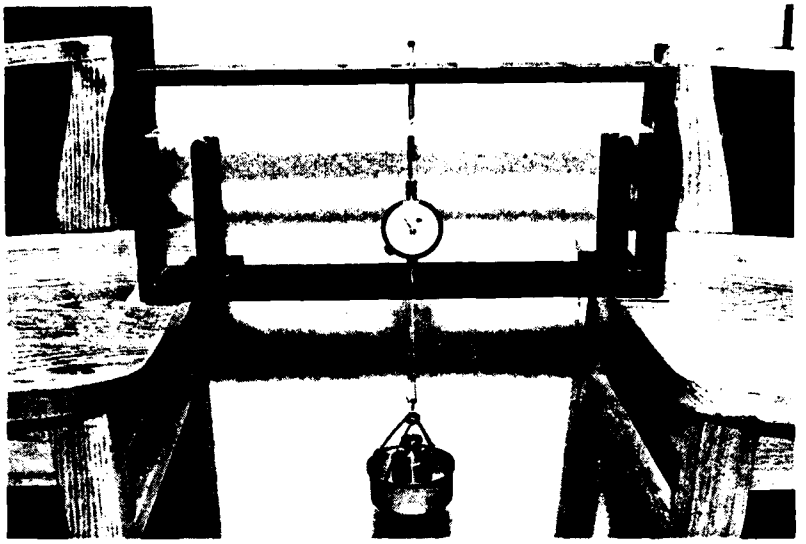

Figure 5

Photograph of a bending stiffness (EI) test. A nominally 2" x 1/8" (5.08 cm x 0.32 cm) aluminum beam is supported within the beam analysis frame on simple supports. It is loaded by a weight at the midpoint between supports, and its midpoint displacement is measured by a dial displacement gauge.

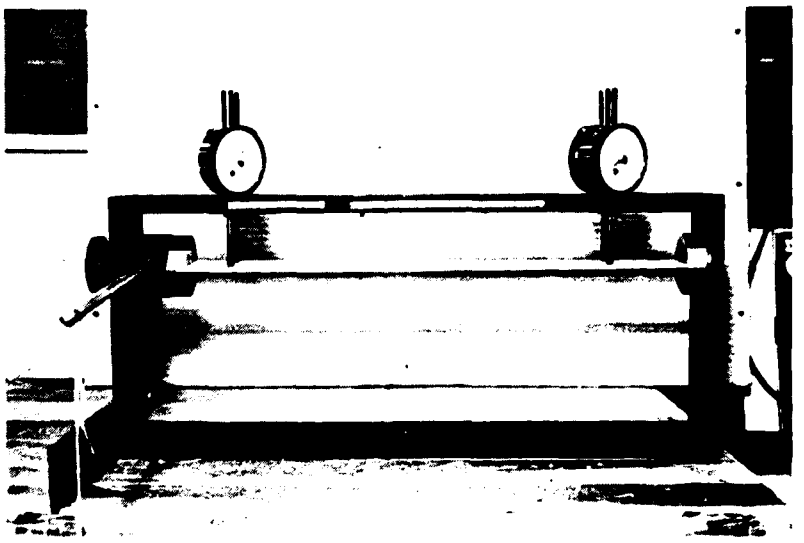

Figure 6

Photograph of a torsion stiffness (GJ) test. A nominally 2" x 1/8" (5.08 cm x 0.32 cm) aluminum beam is held within torque chucks at both ends. The right-hand chuck is fixed to the beam analysis frame, and the lefthand chuck rotates in a bearing about the beam elastic axis. A weight (not shown) hanging from the string applies a torque to the lefthand chuck through the moment arm. The twist deformation between two beam stations is measured by the two pairs of dial displacement gauges.

Figure 7

Photograph of floppy door structure. The shaft clamp is not attached, so the shaft is free to rotate.

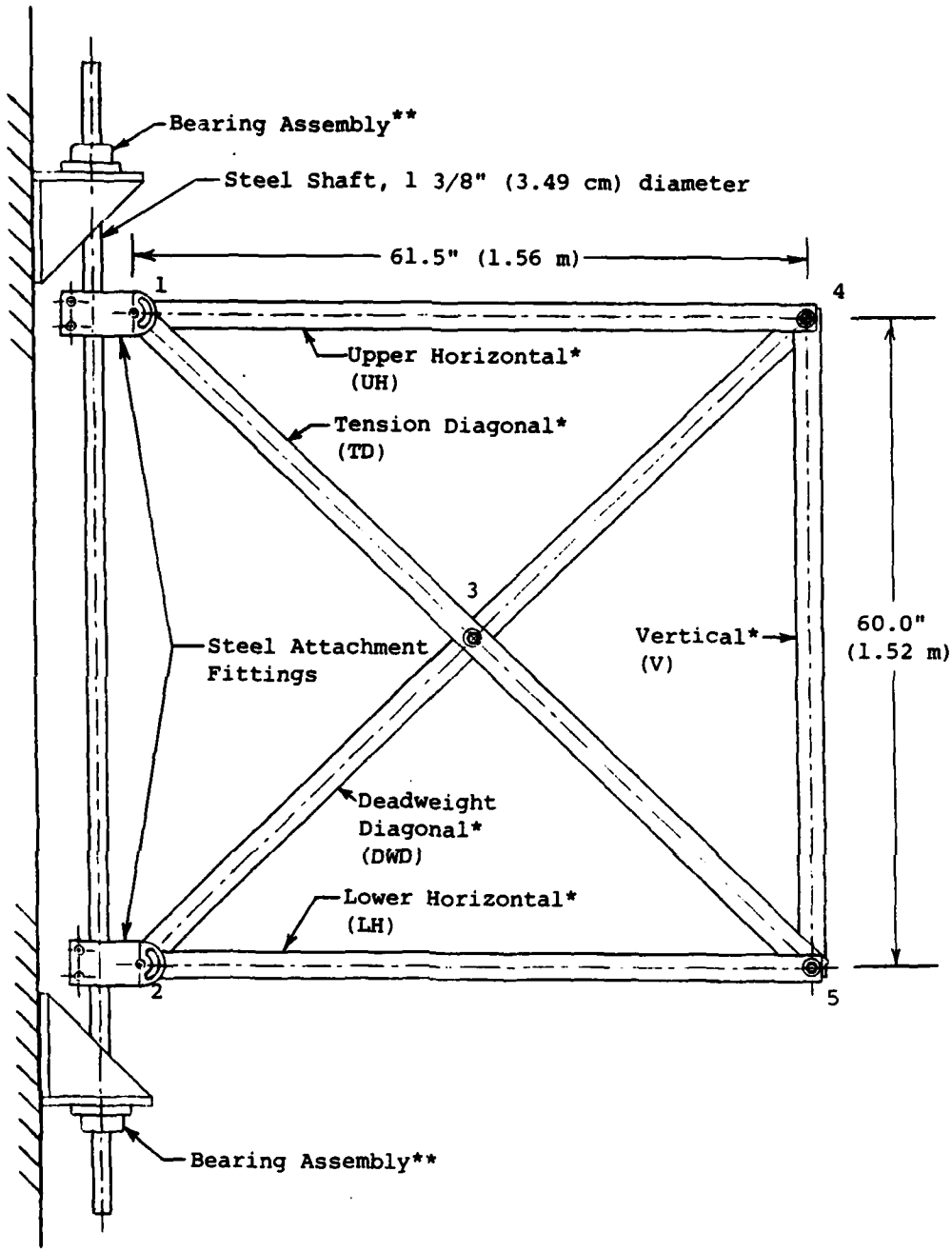

*Aluminum Beam Members
Alloy 6061-T6
Nominal cross-section:
2" x 1/8"
(5.08 cm x 0.32 cm)

**Ball Bearings
Make: SKF
Bearing No. 478207-106
Pillow Block Flange Unit
No. FYP-106
(Bearing seals and all grease were removed to reduce friction.)

Figure 8

Line drawing of floppy door structure.

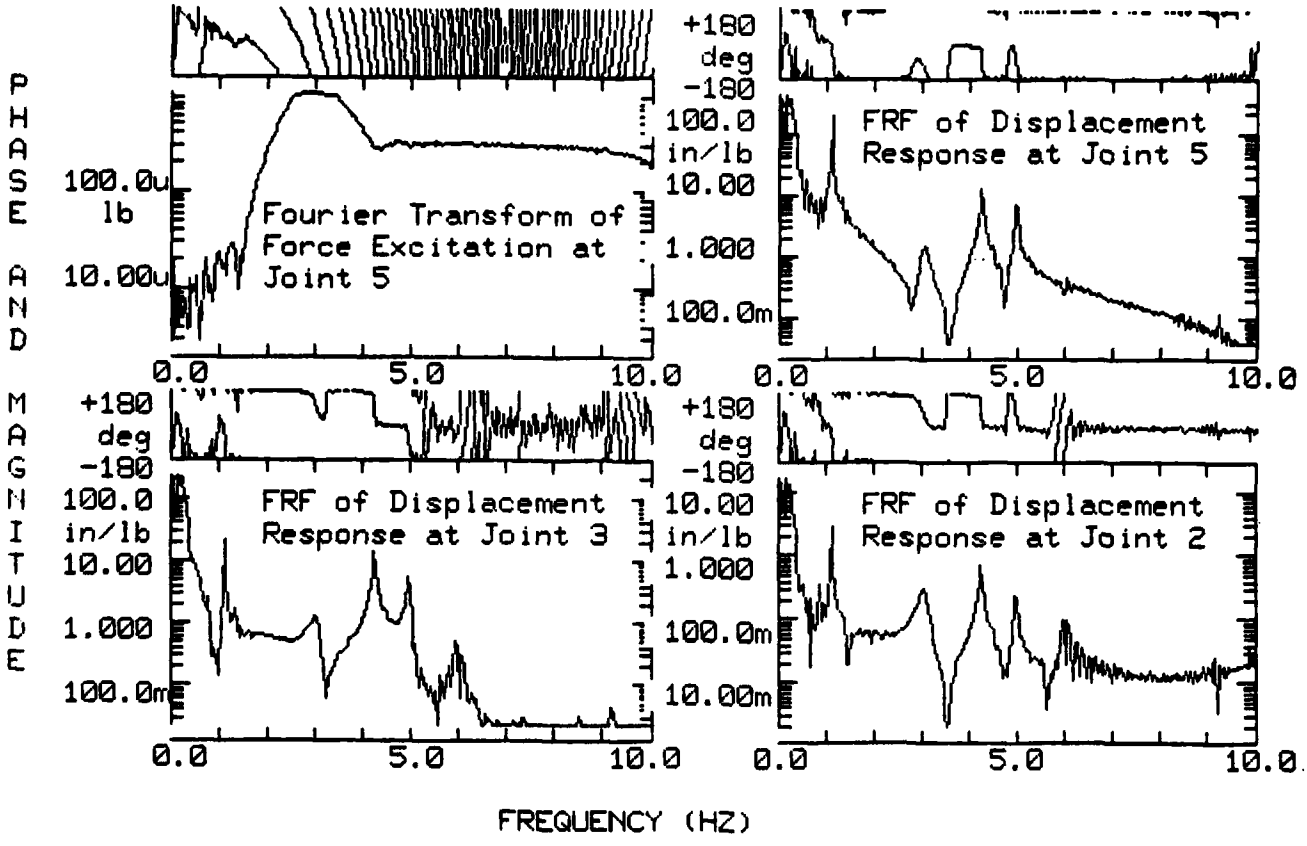

Figure 9

Example of experimental data measured for the floppy door with its shaft free to rotate. The excitation was a single shaped sine chirp with the spectrum shown in the upper left graph. Frequency resolution of the Fourier analysis was 0.04 Hz. The spectra of these graphs were not windowed, but windowing was used in the data analysis, for example to smooth the FRFs in the region of 6 Hz.

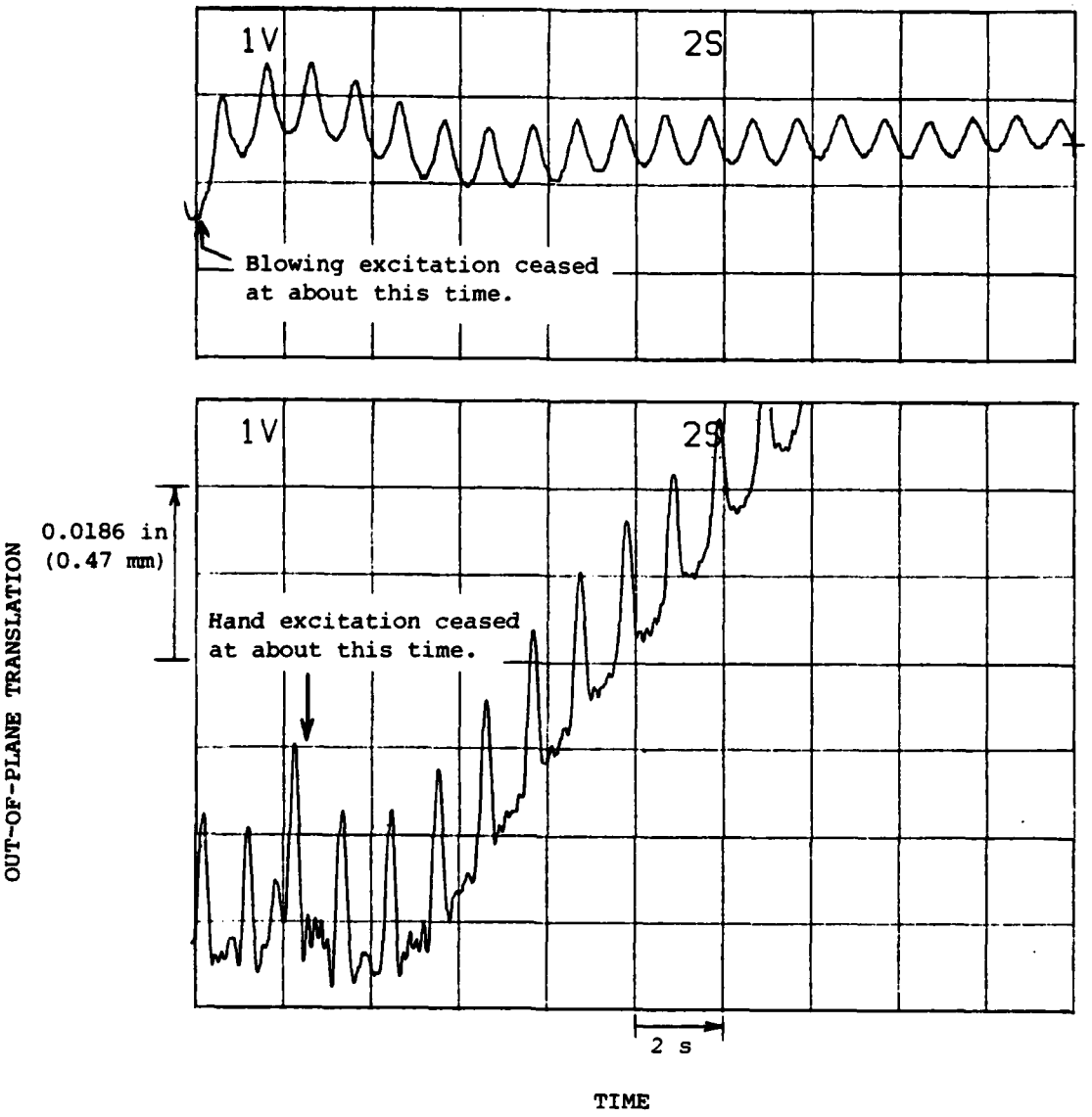

Figure 10

Oscilloscope records of free vibration response at joint 2 following excitation at joint 5 synchronized with the natural frequency of mode 2. The upper record illustrates response below the threshold of visible snapping of the LH member. Even though there was no strong snapping, nonlinearity is clearly evident in the crest-trough waveform shape, especially at the higher levels on the left side of the upper record. The lower record illustrates response with strong snapping of the LH member. The sharp crests correspond to rightward snaps, and the hashy troughs correspond to leftward rebounds near the static equilibrium deformation. The snapping evidently interacted with bearing friction to give the entire floppy door a rightward rigid body rotational velocity, which fell to zero only when the vibration amplitude decayed below the snapping threshold. Note also that the frequency with snapping was lower than the frequency without snapping.

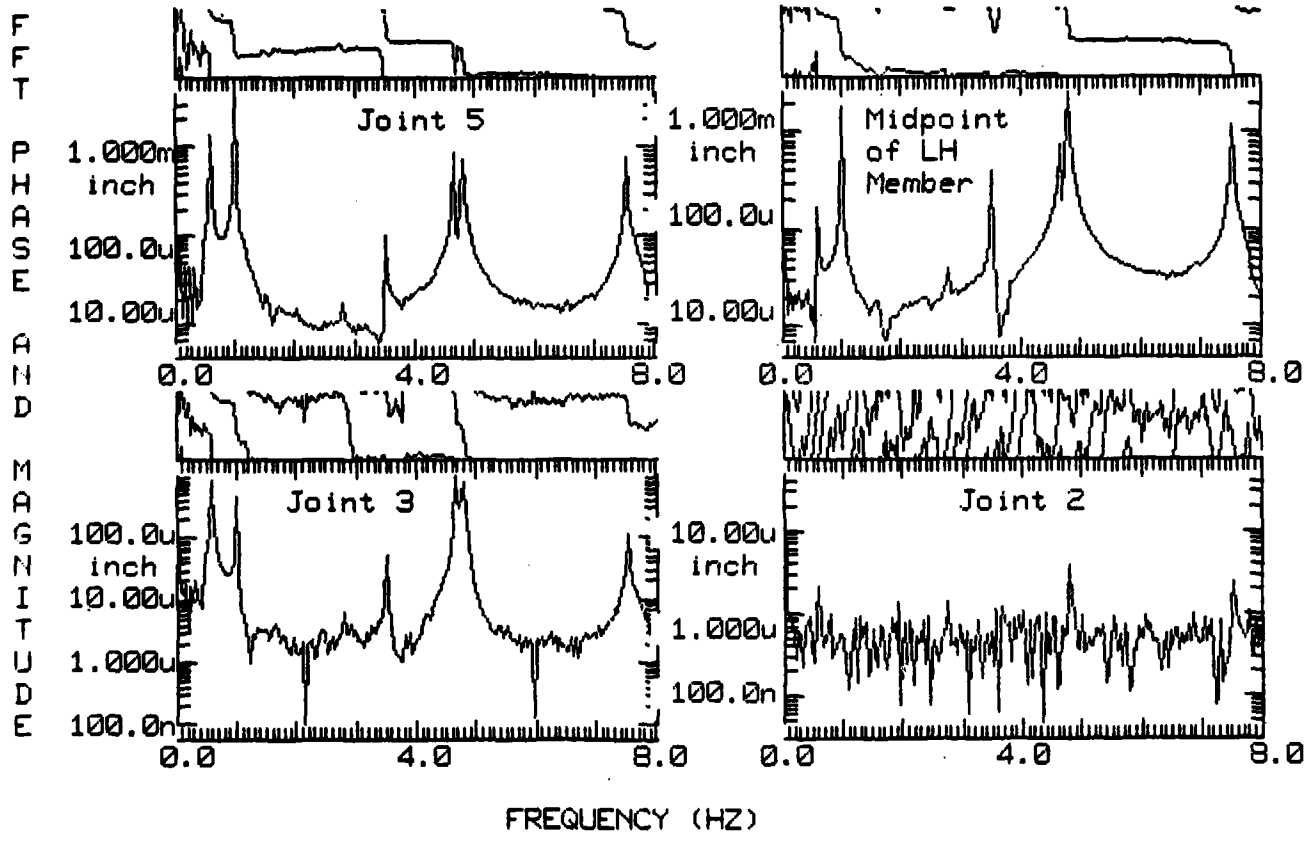

Figure 11

Example (corresponding to Case 5 in Table 3) of experimental data measured for the floppy door with its shaft clamped. The graphs are fast Fourier transforms of free vibration response following a series of gentle taps on the aluminum beams near joint 1 with a padded hammer. Frequency resolution of the Fourier analysis was 0.04 Hz. Data in the lower righthand graph was collected to verify that the shaft was clamped properly.

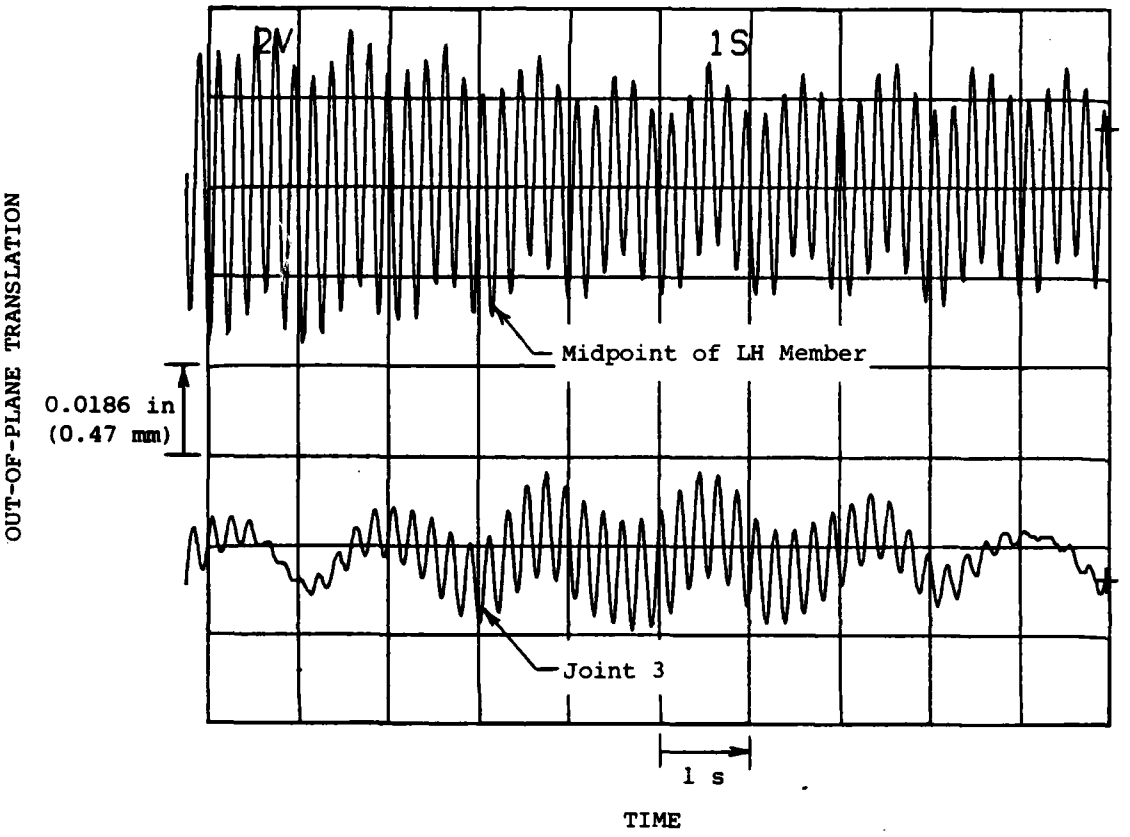

Figure 12

Oscilloscope record of free vibration response of the floppy door with shaft clamped following light oscillatory hand excitation at the midpoint of the LH member. The dominant frequency of the upper trace is 4.79 Hz. On the lower trace, the period between stationary points of the beating oscillation is about 8.5 s, giving 0.12 beat per second, which implies a 0.12 Hz difference between the natural frequencies of modes 4 and 5.

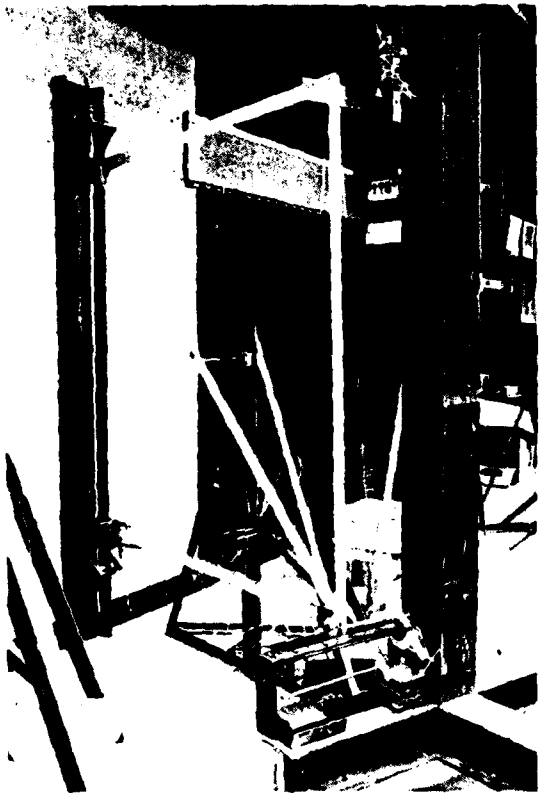

Figure 13

Structure configuration tested for static stability behavior. The weight hanger attached to joint 4 is carrying no weight in this photograph. The rulers used to measure translations of joints 4 and 5 are visible, as is most of the massive wide-flange beam stand to which the rulers were attached.

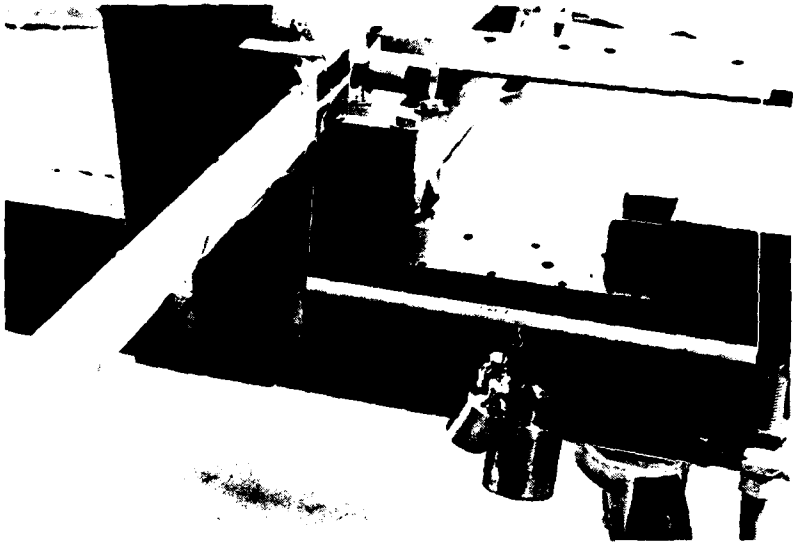

Figure 14

Close-up photograph of lower portion of weight hanger carrying the maximum weight used, 5.5 lb (2.5 kgf). Also shown are joint 5 (with coil) in its extreme deformed position and, behind joint 5, the ruler used to measure the translation of joint 5.

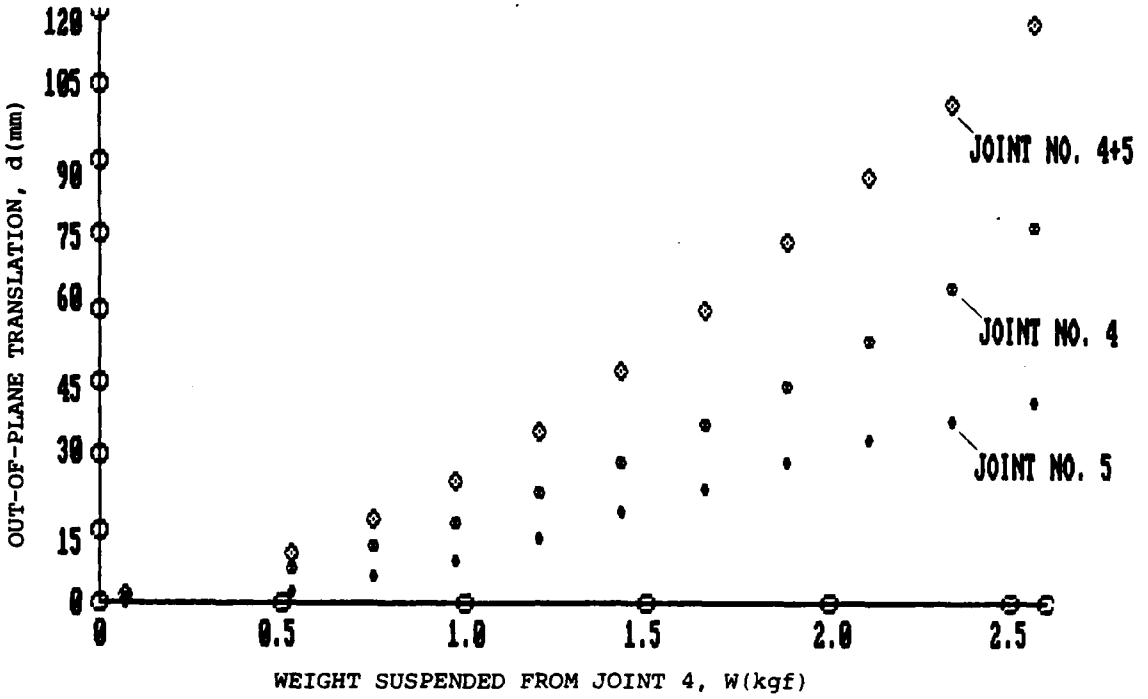

Figure 15

Measured static stability data: out-of-plane translation of joint 4 (leftward) and joint 5 (rightward) due to weight suspended from joint 4.

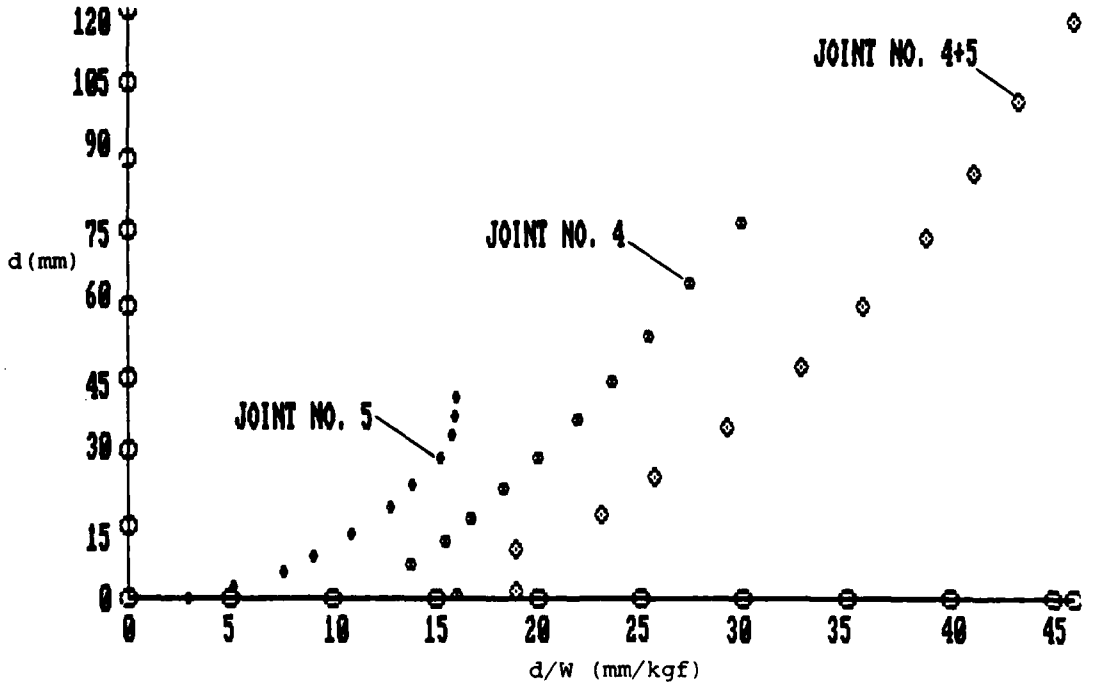

Figure 16

Southwell plots of data from Figure 15.

APPENDIX A

A DIGITAL CONTROL SYSTEM FOR THE VPI ACTIVE STRUCTURAL DAMPING EXPERIMENT

SEPTEMBER 30, 1985

ANTHONY J. KUBIS, JR.

HR TEXTRON INC.
SYSTEMS ENGINEERING DIVISION
2485 McCabe Way
Irvine, California 92714
(714) 660-0253

INTRODUCTION AND SUMMARY

This report describes the analysis of a digital control system for the VPI active vibration suppression experiment. The results of this analysis show that the previously developed analog controller can be converted to a digital design without major changes; and it provides good performance down to a sampling rate of 15 Hertz. A digital redesign is required below that threshold, due to the interactions of the controller with the vibration modes.

The test article consists of a grill-like structure that hangs from a pivoted overhead support bar. Five voice coil actuators apply control forces to the structure and five velocity sensors provide measurements for the control system. The sensors and actuators are colocated on the structure. The controller damps the first six modes on the structure and hence improves the damping characteristics of the structure. Further details concerning the experiment setup can be obtained from References 1 and 2.

Earlier versions of the experimental setup used an analog control system to suppress vibration in the VPI structure. The analog controller is effective at reducing structural vibrations, but implementing and changing an analog control system can be a difficult and time consuming task. Any parameter changes require physically replacing electronic components in the system. The variation in electronic component tolerance can also prove difficult when developing a controlled experimental environment. A natural alternative to the problems associated with an analog controller is to develop a digital control system. The digital controller developed in this analysis can be implemented using

a PC-1000 array processor.

The PC-1000 Desktop Array Processor developed by Systolic Systems Inc. in conjunction with the required IBM PC computer is an excellent addition to the experimental test setup. The PC-1000 array processor performs one specific operation of multiplying a constant 48 x 48 coefficient matrix by a time varying 48 x 1 vector. Since a state space representation of a digital control system involves identically the same operation, the array processor is well suited to this problem. The processor includes analog-to-digital processing of up to 16 inputs and digital-to-analog processing of up to 16 outputs so there is adequate capability to handle the current requirements and allow for future expansion as needed. The processor is capable of sampling in real time at a rate as high as 2000 Hertz. Since this sampling rate is substantially higher than the controlled bandwidth, the array processor should be able to emulate analog control laws equally well without the cumbersome problems previously associated with these controllers.

DIGITAL CONTROL STATE EQUATIONS

The dynamics of the pendulous plane grid are assumed to be given by:

$$[M]\ddot{X} + [D]\dot{X} + [K]X = [B]u \qquad (1)$$

$$\dot{y} = [C]\dot{X} \qquad (2)$$

Where [M], [D] and [K] are mass, damping and stiffness matrices, respectively. X represents the vector of physical displacements of the nodes. [B] and [C] are the control and observation matrices, respectively. $\dot{y}$ is the observation vector

and u is the control vector. Equation (2) represents the fact that only velocity sensors are used.

The transformation between modal coordinates, q, and physical coordinates, X, is:

$$X = [\phi]q \tag{3}$$

which has the following properties:

$$[\phi]^T[M][\phi] = [I] \tag{4}$$

$$[\phi]^T[K][\phi] = [w^2] \tag{5}$$

where [I] is an identity matrix, $[\phi]$ represents the mode shapes and $[w^2]$ is a diagonal matrix whose elements are the square of the natural modal frequencies.

Using the above transformation, Equations (1) and (2) can be written as follows:

$$\ddot{q} + [2\xi w]\dot{q} + [w^2]q = [\phi]^T[B]u \tag{6}$$

$$\dot{y} = [C][\phi]\dot{q} \tag{7}$$

where $[2\xi w] = [\phi]^T[D][\phi]$ and is assumed to be diagonal and ξ is the damping ratio.

The previous equations can be written in state space form by using the vector notation:

$$x = \begin{bmatrix} \dot{q} \\ q \end{bmatrix} \tag{8}$$

where x represents the state vector. Using Equation (8) and rewriting Equations (6) and (7), we obtain the state equations:

$$\dot{x} = [A_c]x + [B_c]u \tag{9}$$

$$\dot{y} = [C_c]x \tag{10}$$

where

$$[A_c] = \begin{bmatrix} -[2\xi w] & -[w^2] \\ [I] & [0] \end{bmatrix} \tag{11}$$

$$[B_c] = \begin{bmatrix} [\phi]^T[B] \\ [0] \end{bmatrix} \tag{12}$$

$$[C_c] = \begin{bmatrix} [C][\phi] & [0] \end{bmatrix} \tag{13}$$

and [0] is the zero matrix.

To obtain the digital state equations, Equations (9) and (10) must be integrated from t_k to t_{k+1}. The resulting digital state equations are:

$$x(t_{k+1}) = [A_d]x(t_k) + [B_d]u(t_k) \tag{14}$$

$$\dot{y}(t_k) = [C_c]x(t_k) \tag{15}$$

where

$$[A_d] = e^{[A_c]\Delta t} \tag{16}$$

$$[B_d] = \left[[A_d] - [I]\right] [A_c]^{-1}[B_c] \tag{17}$$

and $\Delta t = (t_{k+1} - t_k)$

CONTROL LAW

The following form of control will be assumed:

$$u(t_k) = -[K_c]\hat{q}_c(t_k) \tag{18}$$

where $[K_c]$ is the control gain matrix and $\hat{q}_c(t_k)$ is an estimate of the modal velocity of the control modes.

When developing a digital control law, the concept of modal damping becomes difficult to visualize and realize from the sampled form of the control equations. This problem is due to the transformations required to obtain the digital state equations from the continuous state equations. In an attempt to preserve the required modal damping, the control law developed for the continuous case was tested to determine how well it performed in the digital environment. From the results given in Reference 2, the control gain matrix is determined to be:

$$[K_C] = \left[[\phi_A]^T[\phi_A]\right]^{-1}[\phi_A]^T \left[\begin{matrix}[2\xi_A w]_C \\ [0]\end{matrix}\right] \quad (19)$$

Where $[\phi_A] = [\phi]^T[B]$ and ξ_A is the desired active damping ratio.

ESTIMATION LAW

The following form of estimation will be assumed:

$$\hat{q}_c(t_k) = [K_E]\dot{y}(t_k) \quad (20)$$

Where $\hat{\dot{q}}_c(t_k)$ is an estimate of the modes to be controlled and $\dot{y}(t_k)$ is selected since only rate information is available. The estimator derived for the continuous system is dependent on the observation matrix, $[C_c]$. Since the output equation is not altered by the digital transformation, the estimator derived in the previous analysis should work as well for the digital controller. From Reference 2, the estimator is derived as follows:

$$[K_E] = \left[[I] \quad [0]\right] [\phi_o]^T \left\{[\phi_o][\phi_o]^T\right\}^{-1} \quad (21)$$

Where $[\phi_o] = [C][\phi]$.

CONTINUOUS CONTROL LAW ANALYSIS

While developing the digital control law, the continuous control law design will be used as the foundation for determining the performance of the digital control design. The continuous control law design was completed previously (Reference 2). Since completing this analysis, the VPI experiment structural data changed slightly making it necessary to redo the analysis using the updated data.

The control and estimator matrices were recalculated assuming a desired damping of 0.1 in the first six structural modes. Using Equations 19 and 21, the control and estimator matrices were

recomputed and they are given in Table 1. The matrices calculated using the updated structural data are very similar to those calculated in the previous analysis. This can be expected since the changes in structural data were not substantial. Using the updated gain and estimator matrices, the closed loop analysis was redone using the updated structural data. The open loop and closed loop performance for the continuous control system design are given in Table 2. The results indicate that the performance is essentially identical to the earlier analysis and that the general conclusions concerning the system performance are still valid.

These results will be used as the foundation for judging the performance of the digital control system. At high sampling rates, the digital control system should produce results nearly identical to the continuous control case. The highest sampling rate of the PC-1000 Array Processor of 2000 Hertz is better than two orders of magnitude greater than the controlled modes, hence the array processor should be able to emulate a continuous control system. The word lengths available for input-output and data processing should be adequate so that quantization should not be a problem.

TABLE 1

CONTROLLER AND ESTIMATOR MATRICES

Controller Gain Matrix $[K_C]$

$$K_C = \begin{bmatrix} -0.0088 & -0.0015 & 0.0388 & 0.0496 & -0.0412 & 0.1217 \\ -0.0128 & 0.0057 & 0.0366 & -0.0499 & -0.0991 & -0.0027 \\ -0.0092 & 0.0211 & -0.0274 & 0.0763 & 0.0068 & -0.0487 \\ -0.0065 & -0.0046 & 0.0271 & 0.0850 & 0.0717 & 0.0180 \\ -0.0092 & 0.0180 & -0.0230 & -0.0222 & 0.0755 & 0.1426 \end{bmatrix}$$

Estimator Gain Matrix $[K_E]$

$$K_E = \begin{bmatrix} -0.0120 & -0.0176 & -0.0126 & -0.0090 & -0.0126 \\ -0.0013 & 0.0053 & 0.0193 & -0.0042 & 0.0165 \\ 0.0229 & 0.0216 & -0.0161 & 0.0160 & -0.0136 \\ 0.0124 & -0.0124 & 0.0190 & 0.0212 & -0.0055 \\ -0.0094 & -0.0226 & 0.0016 & 0.0164 & 0.0172 \\ 0.0200 & -0.0004 & -0.0080 & 0.0029 & 0.0234 \end{bmatrix}$$

Product or the Control and Gain Matrices $[K_C] \times [K_E]$

$$[K_C] \times [K_E] = \begin{bmatrix} 0.0044 & 0.0012 & -0.0006 & 0.0014 & 0.0014 \\ 0.0012 & 0.0039 & -0.0014 & -0.0020 & -0.0017 \\ -0.0006 & -0.0014 & 0.0028 & 0.0011 & -0.0006 \\ 0.0014 & -0.0020 & 0.0011 & 0.0035 & 0.0008 \\ 0.0014 & -0.0017 & -0.0006 & 0.0008 & 0.0055 \end{bmatrix}$$

TABLE 2

CONTINUOUS CONTROL SYSTEM PERFORMANCE

OPEN LOOP		CLOSED LOOP	
Frequency (Hertz)	Damping (ξ)	Frequency (Hertz)	Damping (ξ)
0.5809	0.0443	0.5826	0.1133
0.8699	0.0287	0.8701	0.0569
1.3489	0.0281	1.3465	0.1040
3.1896	0.0116	3.1948	0.0431
3.4884	0.0059	3.4814	0.0288
4.8499	0.0065	4.8484	0.0304
5.4829	0.0025	5.4828	0.0030
5.6447	0.0021	5.6447	0.0024
5.9516	0.0043	5.9513	0.0069
7.8985	0.0032	7.8987	0.0071
8.1821	0.0041	8.1800	0.0080
9.0058	0.0041	9.0043	0.0106
9.4570	0.0018	9.4562	0.0030
11.2020	0.0020	11.2015	0.0028
12.8670	0.0020	12.8665	0.0040
20.5560	0.0020	20.5560	0.0020
24.0880	0.0020	24.0885	0.0022
26.3700	0.0020	26.3697	0.0024
28.2310	0.0020	28.2306	0.0024
29.8110	0.0020	29.8110	0.0022

DIGITAL CONTROL LAW ANALYSIS

When designing a vibration suppression control system for a flexible structure, it is desirable to increase damping on the structural modes. By observing the damping achieved on the structural modes, we are able to determine the effectiveness of the controller to reduce structural vibration. In the continuous control design, a controller can be designed in a reasonably straightforward manner to improve the damping in specific structural modes since the modal equations remain uncoupled in state space form. When these equations are transformed to digital state space form, Equations 14 and 15, the modal equations, become coupled. Trying to develop a digital controller with a specified set of damping coefficients becomes a difficult task. In an attempt to preserve the required damping while avoiding the complications associated with solving the coupled digital equations, the continuous control matrix is initially used for the digital control system. At high sampling rates, the system should perform as well as the continuous case. At some sampling frequency, the control performance should degrade substantially. The critical sampling rate for this controller can most effectively be determined through analysis.

An analysis of the digital control design was performed using the control and estimator matrices given in Table 1 and the control equations, Equations 14 and 15. Several sampling rates were selected between 10 and 2000 Hertz to examine the effect of the sampling rate on system performance. Table 3 gives the modal frequency and damping characteristics for 10, 20 and 1000 Hertz sampling frequencies. The results indicate that at 1000 Hertz

TABLE 3

DIGITAL CONTROL SYSTEM PERFORMANCE

CLOSED LOOP

SAMPLING=10 Hz		SAMPLING=20Hz		SAMPLING=1000 Hz	
Frequency (Hertz)	Damping (ξ)	Frequency (Hertz)	Damping (ξ)	Frequency (Hertz)	Damping (ξ)
0.5899	0.1120	0.5863	0.1131	0.5826	0.1133
0.8765	0.0560	0.8734	0.0568	0.8702	0.0570
1.3912	0.0996	1.3690	0.1041	1.3470	0.1040
3.2637	0.0249	3.2407	0.0372	3.1958	0.0431
3.5536	0.0163	3.5253	0.0268	3.4823	0.0289
5.0000	***	4.9252	0.0229	4.8502	0.0305
5.4849	0.0024	5.4850	0.0028	5.4829	0.0031
5.6456	0.0021	5.6457	0.0023	5.6447	0.0024
5.9594	0.0039	5.9625	0.0052	5.9516	0.0069
7.9030	0.0025	7.9212	0.0042	7.8995	0.0071
8.1857	0.0034	8.2057	0.0050	8.1808	0.0080
9.0075	0.0034	9.0492	0.0048	9.0060	0.0106
9.4572	0.0018	9.4650	0.0019	9.4565	0.0030
11.2020	0.0021	11.2069	0.0019	11.2018	0.0028
12.8713	0.0022	12.8780	0.0018	12.8675	0.0040
20.5558	0.0020	20.5558	0.0020	20.5558	0.0020
24.0891	0.0020	24.0890	0.0020	24.0889	0.0022
26.3710	0.0020	26.3716	0.0020	26.3705	0.0024
28.2311	0.0020	28.2347	0.0020	28.2317	0.0024
29.8111	0.0020	29.8125	0.0020	29.8116	0.0022

*** denotes unstable mode

there is no degradation in performance when compared to the continuous controller. This is expected since the sampling rate is 200 times higher than the frequency of the first six controlled modes. At 20 Hertz, the performance remains very good and this is not totally unexpected since the sampling-to-control frequency ratio is still four. Theoretically, the sampling rate should remain at least twice the desired control frequency. Several interesting observations can be made from the 20 Hertz case:

1) The modes with frequencies above the sampling rate have damping equivalent to the open loop case as should be expected.
2) Modes between 5 Hertz and 20 Hertz interact with the controller to have a slightly adverse effect on the damping. This is a complex interaction since there is an interaction between closely spaced modes and the digital sampling.
3) The controlled modes show no major changes in performance.

Once the control frequency is reduced to 10 Hertz, the sixth mode goes unstable. The corresponding root is observed in the z-transform analysis to be just slightly outside the unit circle. Ten hertz corresponds to twice the highest controlled frequency and it is theoretically the lowest sampling frequency that should be used. This instability is caused by the modal and sampling interaction noted earlier in the 20 Hertz case. The two lower modes also show a reduction in damping by 50 percent. Although, this control matrix gives unacceptable performance, the

controller could be redesigned to stabilize the system. However, difficulties as noted earlier are in realizing selected levels of damping using a digital analysis. This analysis also demonstrated that a sampling rate of 15 Hertz gives results very similar to those of the 20 Hertz case, and it is the lowest acceptable sampling rate for this control law.

Time simulation runs were also made to demonstrate performance of the control system design. Figure 1 gives the response at the location of the sensors for a 20 Hertz sampling case. The initial modal displacements and rates were set to zero except for initial rates on the first five mode. The five rates were set in a deterministic manner so that the initial observations were all set to one inch/sec. Figure 2 gives the displacements and rates for the first three modes. Comparing these results to those given in Table 3 shows that there is full agreement in the results.

PC-1000 PARAMETER REQUIREMENTS

To implement the controller into the PC-1000 Array Processor requires that the control and estimator matrices be written into a form compatible with the processor. The array processor is capable of processing the following matrix equation:

$$\begin{bmatrix} U_{16x1} \\ X1_{32x1} \end{bmatrix} = \begin{bmatrix} [F11]_{16x16} & [F21]_{16x32} \\ [F12]_{32x16} & [F22]_{32x32} \end{bmatrix} \begin{bmatrix} Y_{16x1} \\ X0_{32x32} \end{bmatrix} \qquad (22)$$

Where U is the actuator input vector, Y is the sensor output vector, X0 and X1 are the present and future internal states and the subscripts indicate the dimensions of the matrices. From Equations 18 and 20 the required equation that must be solved by

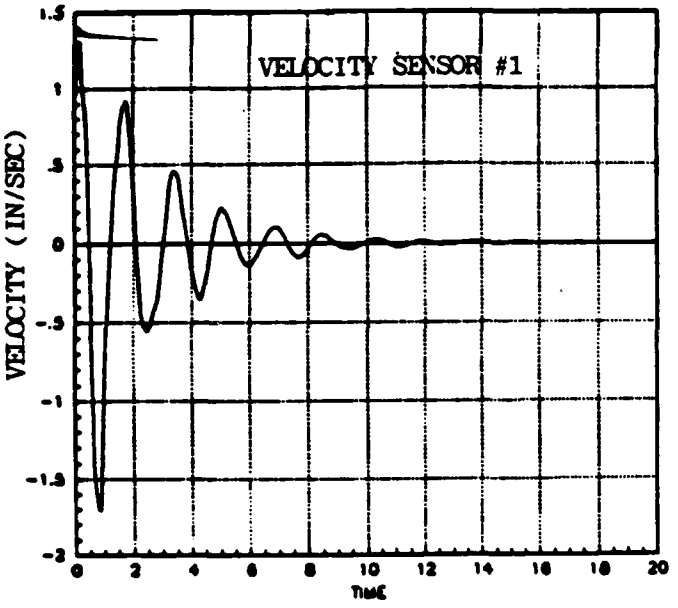

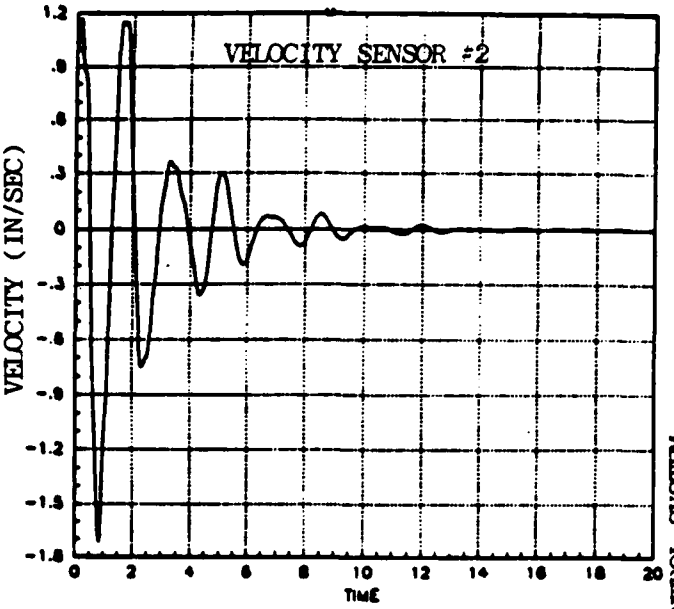

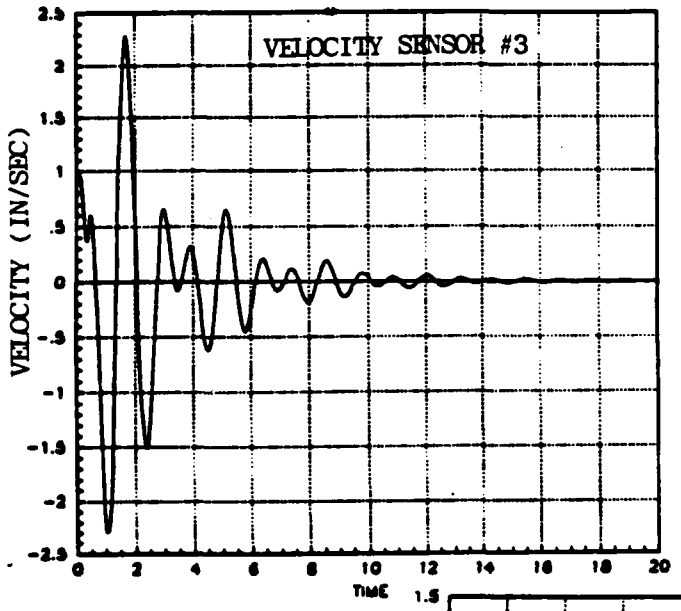

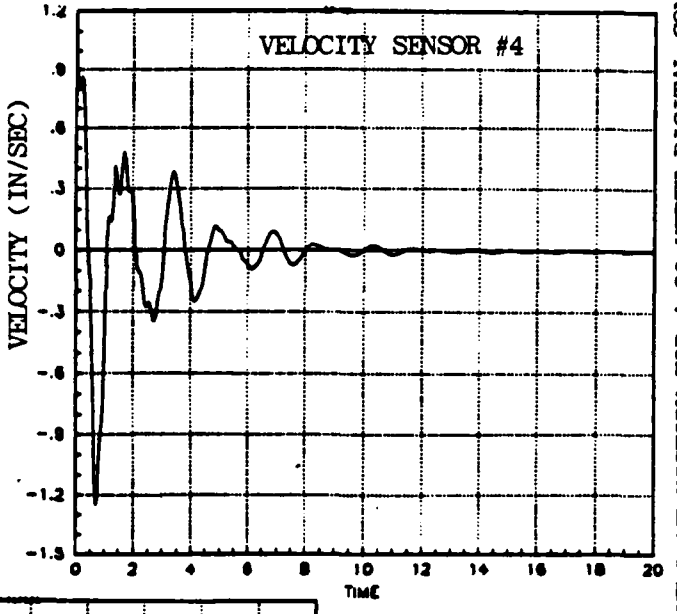

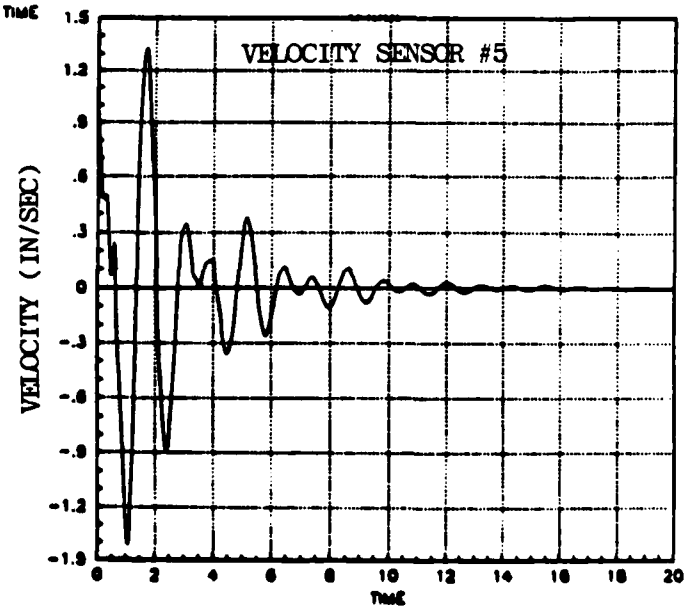

FIGURE 1. OUTPUT TIME HISTORY FOR A 20 HERTZ DIGITAL CONTROL SYSTEM

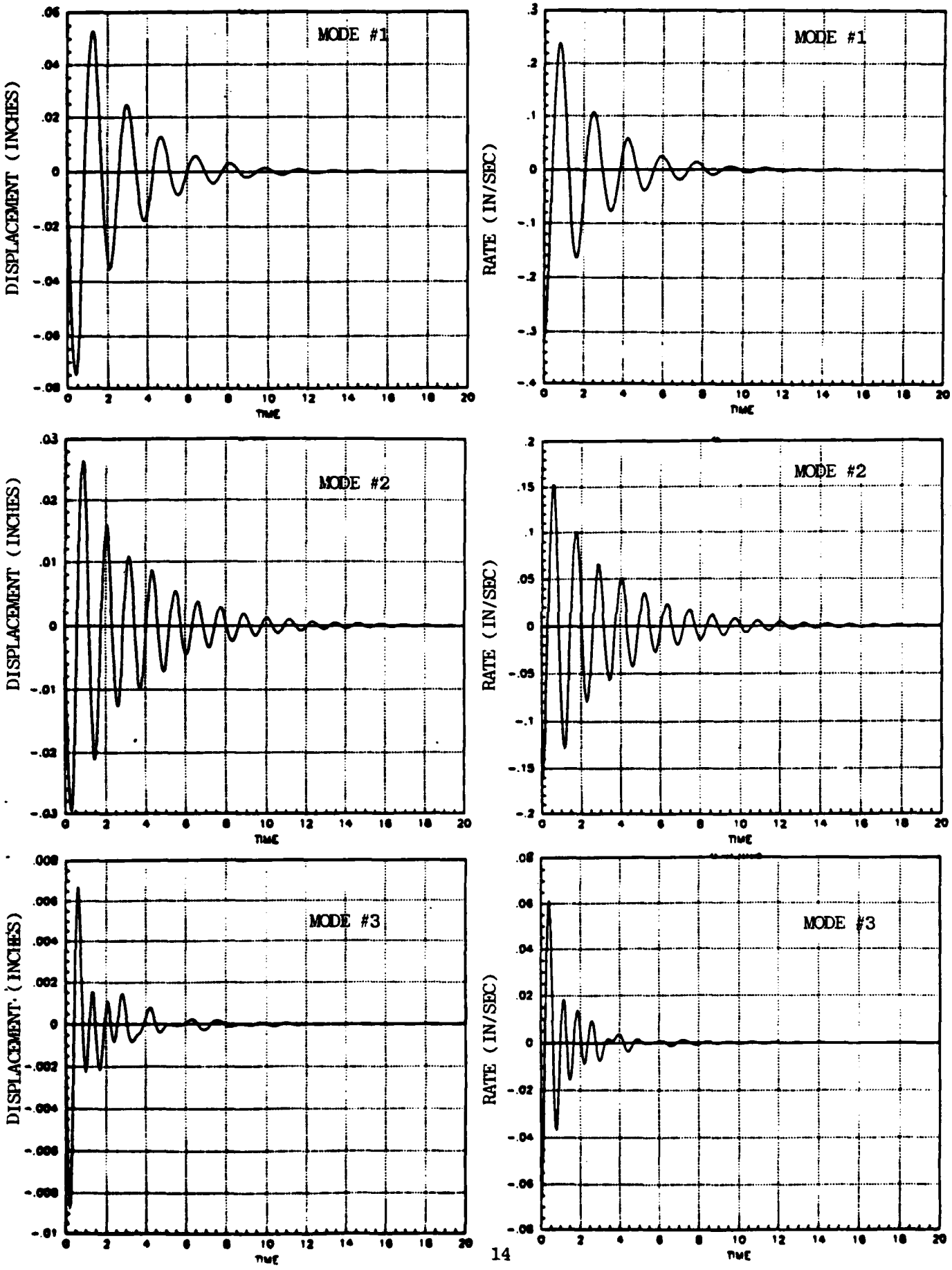

FIGURE 2. DISPLACEMENTS AND RATE OF THE FIRST THREE STRUCTURAL MODES (20 HERTZ SAMPLE RATE)

the array processor is as follows:

$$u(t_k) = -[K_C][K_E]\ y(t_k) \tag{23}$$

where $[K_C]$ and $[K_E]$ have been defined in Table 1. From Equations 22 and 23, $U = u(t_k)$, $Y = y(t_k)$ and [F12], [F21] and [F22] are zero matrices. The [F11] matrix is defined as follows:

$$[F11] = \begin{bmatrix} -[K_C][K_E] & [0]_{5x11} \\ [0]_{11x5} & [0]_{11x11} \end{bmatrix} \tag{24}$$

where the product $[K_C][K_E]$ is defined in Table 1 and [0] is the zero matrix with dimensions defined by the subscripts.

CONCLUSION

The result of this analysis is a digital control system design based on the results obtained from the continuous design analysis. The advantage of this design is that the damping can be set in a reasonably straightforward manner. The results indicate excellent performance down to 15 Hertz. The theoretical limit, 10 Hertz, produces an unstable system using this design. The 10 Hertz limit corresponds to twice the frequency of the controlled modes. A stable system may be achievable at 10 Hertz using digital design methods but the trade-off is a substantially more difficult design problem. Comparing the advantages and trade-offs between both methods, the method of attack chosen seems to be the best one suited for this problem.

In the interest of gaining further insight into this problem, work is currently being conducted to stabilize the system with adequate damping at 10 Hertz using digital design methods. This analysis will be completed and reported in the final report.

REFERENCES

1. Hallauer, William L. Jr., "Experimental Study of Active Vibration Control", Final Report, VPI & SU, 1985.

2. Nayak, Arun P., "Development of an Alternate Control Law for the VPI Pendulous Plane Grid", Final Report, HR Textron, 1984.

APPENDIX B

AN EVALUATION OF DISCRETE-TIME CONTROL FOR ACTIVE STRUCTURAL DAMPING

DECEMBER 2, 1985

ANTHONY J. KUBIS, JR.

SPARTA, INC.
AEROSPACE VEHICLE SYSTEMS DIVISION
23293 So. Pointe Dr.
Laguna Hills, California 92653
(714) 830-6612

INTRODUCTION AND SUMMARY

In recent years, digital computing has appeared in almost every aspect of consumer, industrial, and governmental product development. Recent advances in digital computing capability has resulted in products and ideas that were not possible just a few years ago. Digital computers have developed well established roots in the control of spacecraft. Every spacecraft developed today goes through an evaluation stage to determine if the control system should be an analog or a digital design. In almost every case, the control system is selected to be a digital design. With the advent of large space structures that require active structural damping, it is only natural to evaluate the impact of digital computers on this class of controllers. The purpose of this report is to determine the impact of digital computing on active structural damping and also develop a digital control design to suppress structural damping in the VPI experimental setup.

Digital computers are used in control applications to perform control law implementation, data processing and executive tasking functions. The mathematical equations that define the control laws are implemented in the spacecraft computer. These equations are direct implementations of the control equations tested and defined in a performance verification simulation of the spacecraft. The computer is also used to process sensor input data to convert it into a form acceptable for input to the control laws and to process output data from the control law computations to the actuators. The executive functions include determination of the operational status of the spacecraft,

selecting the appropriate control laws for execution and determination of the actuator/sensor data processing required based on the operational state and subsystem interfacing with the other systems.

This report also presents the results of an analysis of a digital control design for the VPI experiment. The analysis complements the general discussion of digital control by demonstrating through example some of the issues related to suppressing vibration using a digital controller.

This report reveals that substantial investigation is still required to improve the synthesis techniques used for digital vibration suppression control. In addition to the normal problems associated with analog vibration suppression control theory, the synthesis of damping algorithms for a digital controller is very difficult because the concept of damping in an analog system can not be readily transformed into the digital domain. Since damping is not generally realizable in digital analysis, the current solutions include various pole placement techniques or using an analog design for a digital controller and providing a sampling rate higher than the theorical limit of twice the highest controlled frequency. It is obvious that these short term solutions will become inadequate as the complexity of the systems continue to increase. Increases in system complexity will also be limited by digital hardware constraints on sampling rates, memory size, and other factors. Despite the disadvantages of sampled data control, there are some very important advantages favoring digital designs, including the capability of doing on-orbit

parameter adjustments and control law modification. These and other considerations favor the selection of digital over analog vibration suppression systems for most applications.

CURRENT TRENDS OF LARGE SPACE STRUCTURES

With the advent of flexible space structures has come an unprecedented increase in spacecraft control system complexity. Generally, space structures have been considered to be rigid structures so the number of inputs required by the controller has been limited, since these controllers have only been required to perform attitude and velocity control and orientation of the appendages. Current and near-term future payload requirements of many NASA and DOD programs demand space structures that are very large or payloads that must be pointed very accurately. Both classes of structures must be considered flexible since the rigid-body assumptions may no longer be valid. Controlling a flexible structure will result in substantially more inputs to the controller since vibration suppression and shape control must also be performed. As payload requirements become more stringent, the number of inputs required by the controller for military spacecraft will continue to increase. As Figure 1 indicates, the current projections are that the number of inputs required by the controller for military spacecraft will increase exponentially through the year 2000.

A review of the technology models for NASA and DOD also verifies the trend toward large and flexible space structures that require substantially more inputs to the controller. Large space structures are important for applications such as

CONTROL COMPLEXITY TRENDS

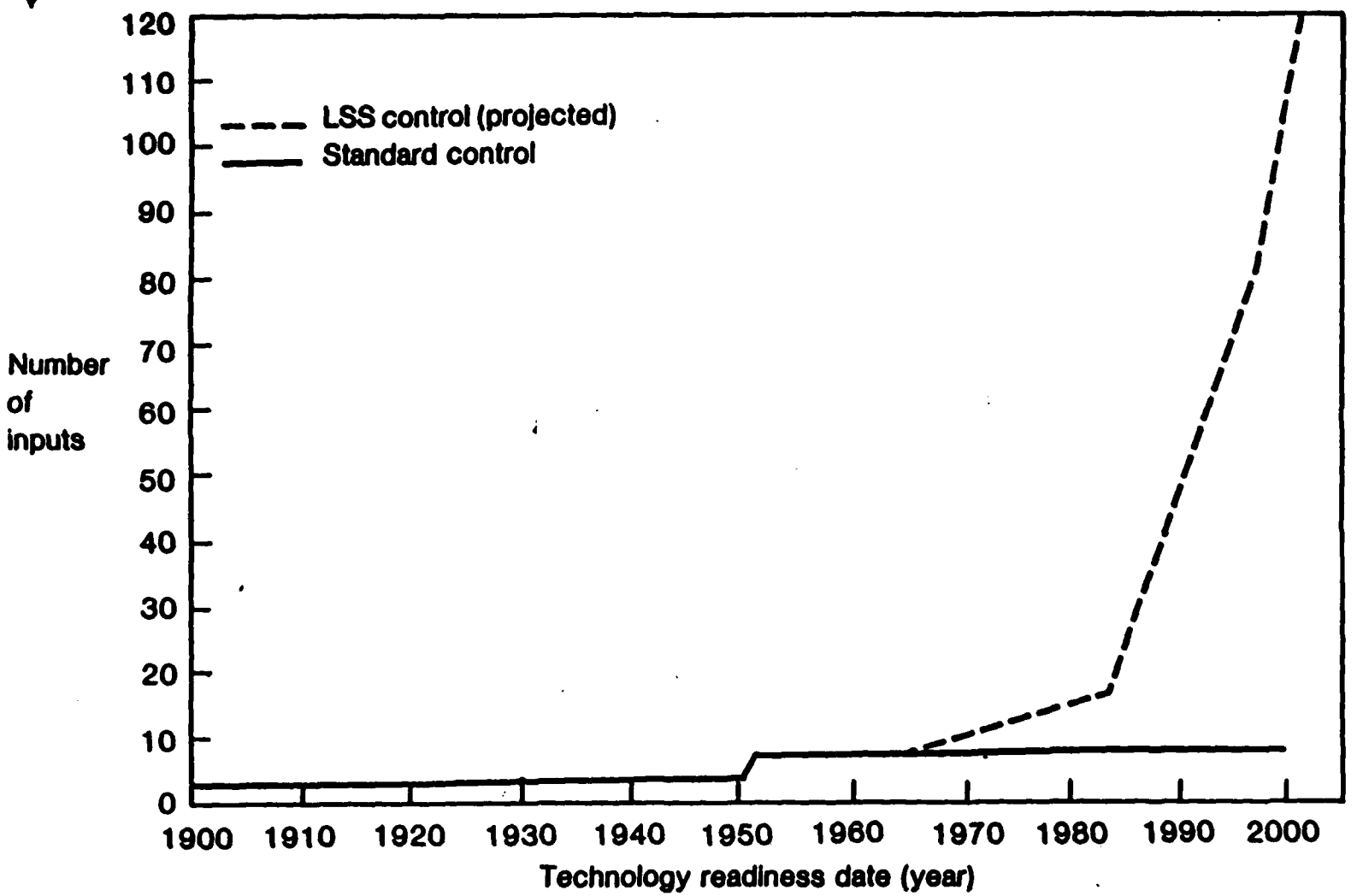

FIGURE 1

(REFERENCE 1)

communications, surveillance, astronomy and space experiments involving high levels of mechanical flexibility (References 2 and 3). These large structures will be flexible because economical considerations dictate that they be collapsible for high-density packaging during launch phase, resulting in deployed structures with low stiffness properties. The DOD requirements also include smaller space structures that must point very accurately. Pointing for many DOD programs will require accuracies through the year 2000 of 10 arcsec down to .1 arcsec, with corresponding stability (jitter) requirements ranging from 1 arcsec down to 0.001 arcsec. Some of the DOD programs have bandwidth requirements as high 2000 Hertz for vibration suppression. Both the DOD and NASA technology models conclude that substantial strides in control and structures analysis capabilities, control hardware development, and test capability need to be developed before these spacecraft can be implemented.

The use of digital computers for controlling large and flexible spacecraft is inevitable. Current development practices will play a role in the development of these systems, and the current trend is toward digital control. Before proceeding with the large space structure issues, we will examine some of the trends of current hardware programs.

CURRENT SPACECRAFT HARDWARE CONTROL LAW IMPLEMENTATIONS

The future trends of developing large space structures will be influenced substantially by current practices. In the past and for most current hardware development programs, structures are treated primarily as rigid bodies. This class of spacecraft

generally requires a three-axes attitude control system with only a few inputs to the controller. In the past these controllers were analog designs, but currently most of the designs are being developed as digital controllers. Typically, these less demanding controllers go through a preliminary assessment to determine if the controller is to be developed as an analog or digital design.

There are several advantages to digital control that ultimately lead the designer to choose it. Current digital design practices dictate that the control laws are generally developed in software while the backup modes of operation are developed as firmware. Software refers to code programmed in Random Access Memory (RAM), while firmware refers to code programmed in Read Only Memory (ROM). This programming practice allows for changes in control parameters and the correction of programming errors from the ground tracking stations. Analog designs may allow selectable gains on certain parameters, but there is no protection against design errors. Selectable gains permit only a limited range of gain parameters. Analog components are also susceptible to parameter drift which may result in an undesirable change in control parameter gains. Digital designs also allow control law implementation that would be difficult or nearly impossible to perform as an analog design. Digital controllers also generally provide better interfacing with other subsystems than analog designs. As an example, a digital controller would interface better with the telemetry, tracking and command, because the TT & C data bus is digital. Analog designs do have certain significant advantages, such as inherent higher levels of radiation hardening and high bandwidth capability. Analog control

should not be completely ruled out since there may be applications where a hybrid analog-digital vibration controller has advantages over a pure digital design.

Generally, the cost of developing a digital attitude controller for current spacecraft programs is approximately the same or slightly higher than the equivalent analog design. As a rule, the cost of generating and qualifying flight software is highly underestimated. A large percentage of the software development cost is due to testing the software. Substantial strides must be made to improve test methods and develop automated code generation methods, before these costs can be substantially reduced.

There are certain applications where multivariable control techniques are required. The practice in these hardware programs has been to employ classical loop-by-loop design procedures beyond their scope. In addition to extending these procedures beyond their limit, analog analyses are often conducted for digital controller designs. Potential design problems are uncovered and corrected by extensive simulation studies.

DIGITAL CONTROL ANALYSIS FOR LARGE SPACE STRUCTURES

Some large space structures will require control systems with multiple inputs and outputs in order to suppress vibration or maintain accurate shape and alignment. The analysis of these multiple input/output control systems is generally performed by representing the system in a state space form. The continuous state space matrices for a large space structure can be easily obtained from the second order dynamics representation for the

structural modes. The analyst must select the modes that will be included in the analysis model. Using a structural analysis program such as NASTRAN, the analyst can obtain the eigenvalues and eigenvectors for the structural model. Damping is generally derived by test performed on the structure or by simple assumption.

The general approach to reducing the vibration in these structures is to increase the level of damping in the modes within a desired bandwidth. Damping can be increased by active damping, passive damping or a combination of both. By definition, the performance of the control system is judged by its ability to provide the desired level of active damping while satisfying other constraints such as power and weight limits.

Obtaining the digital state space representation for a linear system simply requires that we integrate the continuous state space equation over the delta sampling interval. The resulting digital state space equation has a similar form to the continuous equation, but their meanings are very different. The transformation from analog to digital results in a loss in any simple relationship for damping. Basically, the damping concept does not lend itself well to an interpretation in the digital or discrete domain. This conclusion about digital systems presents a serious problem, since the preferred way of representing performance in a vibration suppression control system is by examining the level of increased modal damping. It is possible to do an equivalence conversion of the closed loop digital control system back to the analog domain to obtain the modal damping. This technique has

worked well in the analysis of the digital design for the VPI experimental setup, but it is time consuming and it does not necessarily lead to optimal results.

The control analysis techniques used in the analysis of analog control systems generally have an equivalent counterpart in the analysis of digital systems. The analysis techniques for analog and digital generally complement each other, but ther interpretation is not always the same. At the most fundamental level, stable roots that are in the left-hand plane in Laplace domain will be within the unit circle in the z-transform domain.

The primary methods for developing a digital multi-variable control system for vibration control are pole placement and discrete linear quadratic regulator design. Both techniques can develop stable digital controllers. There are general limitations with these techniques when developing a digital controller for structural vibration control due to the inability to represent damping in digital form. Determining the level of damping in a digital control design requires a conversion back to analog. There is a need to resolve some important issues related to large space structure digital controllers if they are to be used successfully on hardware development programs.

Most of the current issues that limit the development of analog controllers for large space structures also hold true for digital systems. Issues such as a need for better structural modeling techniques, a need for integrated technologies design techniques, etc. will remain important for both analog and digital systems. In summary, the design of digital control systems is plagued by all of the disadvantages of analog systems

with the addition of the digital design problems described above. Even with these design problems, a digital design is very important because of the inherit implementation advantages. When developing digital controllers where the sampling rate is much higher than the control bandwidth, current technology may warrant analog design techniques applied to digital systems as an adequate (not optimal) design methodology.

FUTURE DIGITAL CONTROL IMPLEMENTATION REQUIREMENTS

In addition to the limits imposed in developing digital control systems for large space structures by the analysis capability, there are other constraints that must be considered, such as computational capability. The onboard computer that must perform the control law computations is limited by three primary factors, namely (1) computational speed, (2) wordlength, and (3) memory constraints.

The current state-of-the-art in flight-qualified digital computers is insufficient to handle the demands of many anticipated large space structures. Current computing capability is insufficient in terms of computational speed and memory limitations. The memory required for currently projected large space structures is as high as 40 million bytes (Reference 4). This memory requirement is over two orders of magnitude higher than present day technology. The requirements for processor speed is about three times higher than current capability. The most promising way of closing the gap between computational needs and current technology is through the use of distributed/parallel processing technology.

By using distributed processing, the demand on memory requirements is reduced to a factor of 3 or 4 beyond the current state of the art (Reference 4). Distributed processing would eliminate the discrepancy between the required and current state-of-the-art processor speed. The processing scheme could potentially be a two or three tier hierarchically distributed system. A top level supervisory controller would interface with the ground and supervise the next lower level processors. Each of the the lower level processors would control several lower order control processors.

Work is currently being conducted on a parallel processor dedicated to simulating large flexible space structures (Reference 5). Although these dedicated processors are designed for simulation purposes, the technology could easily be modified for onboard computer applications. (Distributed processing described above represents a specific form of parallel processing.) The simulation processors are expected to reduce simulation execution time substantially. In a benchmark problem that requires 5.09 hours to run on the Cray 1S, the parallel processor is estimated to compute the same problem in 0.30 hours.

In addition to the concerns over flight-computer hardware, the onboard computers for large structure control will require substantial amounts of software. Since the cost of developing software for current systems is extremely high, the cost of developing software for large space systems is a major concern. Much of the software cost is due the testing and verification required before the structure is placed on-orbit. Substantial

work must be done to reduce the cost associated with software testing and verification. Since there will have to be a substantial amount of software developed for these systems, they would benefit greatly for automated software development tools. The current state of the art in automated software produces efficient code; hence, they would be unacceptable for control applications that require a lot of computations running at high sampling rates.

VPI EXPERIMENT DIGITAL CONTROLLER

The VPI digital experimental setup consists of a grill-like flexible structure, five colocated actuators and sensors, and a PC-1000 Desktop Array Processor. The actuators and sensors consist of colocated voice coil actuators and velocity sensors. Since the structure has been used extensively in the past, the structural model has been refined to a reasonable degree of certainty. The array processor performs the input/output data processing required for the sensors and actuators and includes an implementation of the vibration suppression control law. The sampling rate of the array processor is variable up to a sampling rate of 2000 Hertz. Since, the sampling rate of the processor can be set to more than two orders of magnitude higher than the required control bandwidth, the array processor may also be used to execute and test analog control designs in addition to testing digital designs. Further details concerning the VPI experimental test setup can be obtained from References 6, 7, and 8.

A digital compensation scheme consisting of a digital control law and state estimator was developed previously (Reference 8).

The state estimator used in current and the previous digital designs have remained unaltered from an earlier analog design since the estimator worked well in the analog design and there is no transformation required; hence, there should be no degradation in estimator performance. A digital controller was developed previously using a discrete version of the continuous controller designed in Reference 7. Through analysis, it was determined that this controller proved to be effective down to 15 Hertz. Since theoretically a stable controller can be designed to sample at twice the control bandwidth, the objective of the present analysis is to demonstrate that a controller can be designed to operate at the theoretical limit of 10 Hertz. From Reference 8, the sixth mode goes unstable when the previous controller is used at 10 Hertz.

From the previous results obtaining a numerical solution for specified damping, similar to what was used in the analog design, is prohibitively difficult in discrete analysis due to the analog-to-digital conversion of the damping measure. Alternatively, a digital Linear Quadratic Regulator (LQR) design and a digital pole placement were both considered. Digital pole placement was selected since both methods have the disadvantages of being essentially trial and error techniques and they both require digital-to-analog eigenvalue conversion to obtain the level of damping, but pole placement has the advantage of being a computationally quicker operation.

The method of attacking the problem was to use the resulting control gains developed previously and alter the control gains to stabilize the system and improve the overall

performance. The objective was to increase damping in the second, fourth and fifth modes, and to stabilize the sixth mode, providing an adequite level of damping. The analysis was performed by first determining the sensitivity of the control gains, altering those gains that improved the performance, and examining the analog equivalent level of damping in the first six modes. The resulting control gain matrix is given in Table 1.

The performance of the digital control design at 10 Hertz is given in Table 2. The new control gain matrix does stabilize the sixth mode, but the damping levels in the fourth, fifth and sixth modes are still less than the results given in the continuous closed loop design. Varying the control gains did not exhibit any substantial improvement in the level of damping in these three modes. Additional analysis could improve the performance slightly, but substantial improvement in performance does not seem possible. The reduction in performance is probably due to the modes lying near the theoretical control limit of half the sampling rate. There are several modes around this theoretical limit that interact with each other and with the control system.

The results of this analysis indicate stable performance at 10 Hertz, but the degradation in performance warrants selecting a slightly higher sampling rate. Additional improvements in performance might be achieved through other alternatives, such as improving the estimator design. The discrete analysis of the VPI experiment demonstrates the need for improved discrete analysis techniques.

TABLE 1

CONTROLLER AND ESTIMATOR MATRICES

Controller Gain Matrix $[K_C]$

$$K_C = \begin{bmatrix} -0.0699 & -0.0015 & 0.0388 & 0.0496 & -0.0411 & 0.1216 \\ -0.0128 & 0.0116 & 0.0366 & -0.0499 & -0.0988 & 0.0000 \\ -0.0092 & 0.0211 & -0.0827 & 0.0763 & 0.0068 & -0.0487 \\ -0.0065 & -0.0046 & 0.0271 & 0.1701 & 0.0717 & 0.0180 \\ -0.0092 & 0.0180 & -0.0230 & -0.0222 & 0.0755 & 0.0713 \end{bmatrix}$$

Estimator Gain Matrix $[K_E]$

$$K_E = \begin{bmatrix} -0.0120 & -0.0176 & -0.0126 & -0.0090 & -0.0126 \\ -0.0013 & 0.0053 & 0.0193 & -0.0042 & 0.0165 \\ 0.0229 & 0.0216 & -0.0161 & 0.0160 & -0.0136 \\ 0.0124 & -0.0124 & 0.0190 & 0.0212 & -0.0055 \\ -0.0094 & -0.0226 & 0.0016 & 0.0164 & 0.0172 \\ 0.0200 & -0.0004 & -0.0080 & 0.0029 & 0.0234 \end{bmatrix}$$

Product of the Control and Gain Matrices $[K_C] \times [K_E]$

$$[K_C] \times [K_E] = \begin{bmatrix} 0.0052 & 0.0023 & 0.0001 & 0.0020 & 0.0022 \\ 0.0013 & 0.0039 & -0.0013 & -0.0020 & -0.0016 \\ -0.0019 & -0.0026 & 0.0037 & 0.0003 & 0.0001 \\ 0.0025 & -0.0031 & 0.0028 & 0.0053 & 0.0004 \\ 0.0000 & -0.0017 & 0.0000 & 0.0006 & 0.0038 \end{bmatrix}$$

TABLE 2

DIGITAL CONTROL SYSTEM PERFORMANCE

SAMPLING AT 10 HERTZ CLOSED LOOP SYSTEM

PREVIOUS CONTROLLER		CURRENT CONTROLLER	
Frequency (Hertz)	Damping Ratio	Frequency (Hertz)	Damping Ratio
0.5899	0.1120	0.5904	0.1235
0.8765	0.0560	0.8798	0.0646
1.3912	0.0996	1.4092	0.1263
3.2637	0.0249	3.2880	0.0278
3.5536	0.0163	3.5590	0.0183
5.0000	***	4.9655	0.0071
5.4849	0.0024	5.4850	0.0024
5.6456	0.0021	5.6456	0.0021
5.9594	0.0039	5.9590	0.0039
7.9030	0.0025	7.9042	0.0023
8.1857	0.0034	8.1860	0.0033
9.0075	0.0034	9.0072	0.0035
9.4572	0.0018	9.4571	0.0018
11.2020	0.0021	11.2018	0.0020
12.8713	0.0022	12.8708	0.0022
20.5558	0.0020	20.5558	0.0020
24.0891	0.0020	24.0890	0.0020
26.3710	0.0020	26.3708	0.0020
28.2311	0.0020	28.2312	0.0020
29.8111	0.0020	29.8111	0.0020

*** denotes unstable mode

CONCLUSION

By examining current trends in space structure development and the requirements imposed on the controller by large space structures, it is obvious that digital computers will be used for controlling these structures. Currently, the demand on processors is relatively low, so the sampling rate can be set high enough that an analog design can be implemented into a digital design with excellent results. As the demand on the processor increases, and all indications are that this demand will increase substantially, the sampling rates must be decreased to accommodate the large number of computations that must be performed each cycle. The reduced sampling rate will require that the controller be designed using digital design techniques. However, substantial work is still required to improve the digital design techniques for vibration suppression controllers, since there are currently no techniques to directly design multivariable vibration suppression control systems. All of the current design techniques require that the level of damping be observed by an equivalence conversion back to analog.

Digital controllers have certain advantages over analog controllers including the ability to alter the control algorithm on-orbit, implementation of control configurations that would be difficult or impossible to accomplish in analog circuits and easier interfacing with other subsystems. The cost of developing a digital controller may be greater than for an equivalent analog design, but in many cases the advantages of a digital design outweigh the potentially higher cost. It is uncertain whether an

analog or a digital design would be more costly for a large space structure. Because of the advantages of digital control, it is unlikely that vibration controllers will ever be completely implemented in analog. Most of the controllers probably will be design as digital, but there maybe cases where hybrid analog-digital controllers are a better choice. A hybrid design might be selected because of radiation hardening requirements, high bandwidth requirements, and/or cost considerations. Selection of a digital or hybrid design will probably be determined on a case-by-case bases.

REFERENCES

1. Data presented by Dr. John Sesak at the AIAA/DOD Space Systems Technology Workshop; Navigation, Guidance and Control Panel; Spring, 1984.

2. "An Investigation of Enabling Technologies for Large Precision Space Systems", Charles Stark Draper Laboratory, 1982.

3. "NASA Space Systems Technology Model", Fifth Issue, 1984.

4. Data presented by Rex Agler at the AIAA/DOD Space Systems Technology Workshop; Navigation, Guidance and Control Panel, Spring, 1984.

5. Quest Magazine, TRW Electronics and Defense Sector, Volume 8, Number 1, Summer, 1985.

6. Hallauer, William L. Jr., "Experimental Study of Active Vibration Control", Final Report, VPI & SU, 1985.

7. Nayak, Arun P., "Development of an Alternate Control Law for the VPI Pendulous Plane Grid", Final Report, HR Textron, 1984.

8. Kubis, Anthony J. Jr., "A Digital Control System for the VPI Active Structural Damping Experiment", HR Textron, 1985.

END

12-86

DTIC